Review
UDC 546.62:539.26:548.73
DOI: 10.52957/2782-1900-2025-6-3-39-66

METHODS OF TG, DSC, AND SYNCHROTRON ANALYSIS FOR ENHANCING THE REACTIVITY OF ALUMINUM-BASED METALLIC FUELS

V.G. Shevchenko*, D.A. Eselevich, V.N. Krasilnikov, A.V. Konyukova

Vladimir Grigorievich Shevchenko, Doctor of Chemical Sciences; **Danil Aleksandrovich Eselevich**, Candidate of Chemical Sciences; **Vladimir Nikolaevich Krasilnikov**, Doctor of Chemical Sciences; **Alla Vyacheslavovna Konyukova**.
Institute of Solid State Chemistry UB RAS, Russia, 620990, 91, Pervomaiskay St., Ekaterinburg, *shevchenko@ihim.uran.ru, diablohulk@gmail.com, kras@ihim.uran.ru, alla.konyukova.5656@mail.ru*

Keywords: *vanadium-containing hydrogel; activation; oxidation completeness; aluminum; powders; programmable heating*

Abstract. *The paper demonstrates the capabilities of thermal and X-ray phase analysis of the interaction products for developing modification methods of aluminum-based powders. It provides searching for optimal synthesis regimes of new metallic fuels for composite energetic systems of various purposes. The importance and utility of applying considered methods for selection the composition and synthesis conditions of promising materials have been evaluated.*

For citation:
Shevchenko V.G., Eselevich D.A., Krasilnikov V.N., Konyukova A.V. Methods of TG, DSC, and synchrotron analysis for enhancing the reactivity of aluminum-based metallic fuels // From Chemistry towards Technology Step-by-Step. 2025. Vol. 6, Iss. 3. P. 39-66. URL: https://chemintech.ru/en/nauka/issue/6423/view

Introduction

The selection of metallic fuels for energetic condensed systems (ECS) of various purposes is based on the specific heat release characteristics of metals during combustion [1]. Many metals, such as Be, Li, B, Al, and Mg, are of interest in terms of specific heat of combustion (Table 2) [2]. Indeed, beryllium and its reaction products are highly toxic; lithium is unstable under storage and operational conditions. The most widely used powders are those of Al, Mg, and B. However, the issue of the efficient utilisation of metallic fuels and their energy potential to enhance ECS for various applications has not been addressed yet. A lot of recent review articles are discussing the approaches to modification of aluminum powders [3-6]. A logical and effective method to increase reactivity appears to be reducing particle size. For instance, nanosized aluminum powders exhibit very high reactivity [3]. However, their use in solid propellant compositions is challengeable and related to compatibility with fuel binders, their stability during storage, and losses of active metal during processing. Consequently, the most widely used powders are micron-sized aluminum with the maximum possible active metal content, obtained through melt atomisation to produce spherical particles [7]. The cost of such powders is much lower than the cost of Alex Aluminium with a particle size of 120-160 nm [8].

Fig. 1 presents the interaction pattern of microsized Al powders based on the research findings obtained through thermogravimetry (TG), differential scanning calorimetry (DSC), and phase analysis of oxidation products at characteristic heating stages [9].

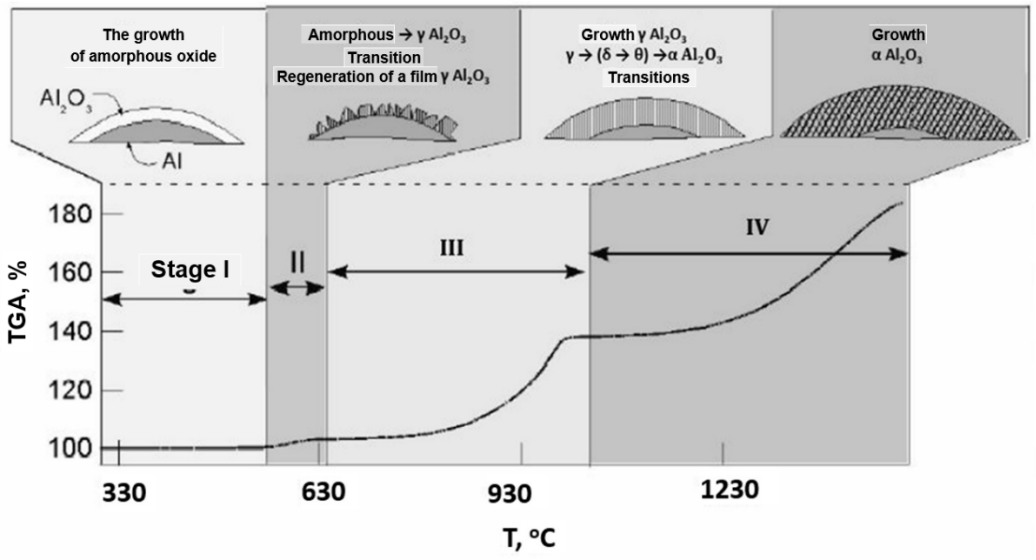

Fig.1. Scheme of aluminum particle oxidation [9].

According to Fig. 1, under conditions of programmed heating in air, temperature intervals can be identified. It corresponds to the acceleration and deceleration of the interaction process. Within these intervals, the aggregate state of Al changes (melting), and transformations occur in the oxide layer on the particle surface. It transitions from an amorphous state to γ- and α-forms of Al_2O_3 as the temperature of the oxidative environment increases. The formation of each crystalline phase on the surface of the dispersed aluminum enables the delivery of oxygen to the zone of chemical interaction. It is associated with a loss of continuity in the protective layer, caused by stresses arising from changes in the crystalline structure of the oxidation products [9]. The low melting point of aluminum and the stresses generated during melting due to the difference in the coefficients of thermal expansion of Al and Al_2O_3 lead to the rupture of the protective film. It ensures oxidiser transportation but simultaneously causes particle agglomeration due to the appearance of liquid aluminum.

Thus, the features of phase formation during the heating of dispersed aluminum in an oxidative environment show the characteristic challenges associated with utilising the energetic potential of Al as a metallic fuel in condensed systems for various applications. These challenges are related to particle coarsening at the moment of liquid Al formation and the high protective properties of Al_2O_3 oxide formed on the particle surfaces. Consequently, to accelerate oxidation, it is necessary to affect on the properties of the products formed during heating in an oxidative environment.

The monograph [10] considers an analysis of the fundamental physicochemical properties of Al melts with rare-earth elements (REEs) and the oxidation characteristics of powders produced from them via atomisation. According to those, the surface properties of particles can be controlled by considering the reactivity and surface activity of alloying elements introduced into the aluminum melt. Due to adsorption processes in surface layers, a surface-active metal becomes concentrated. It leads to an increase in its surface concentration even at low bulk concentrations within the particles. This is related to the difference in surface

tension between aluminum and the alloying additive and is greater when this difference is larger [11]. Additionally, a second factor influencing the reactivity of alloy powders is the oxidation activity of the alloying additive itself. Research in this direction allowed the author of [11] to develop a scheme of the oxidation mechanisms for Al particles doped with active elements. Scheme in Fig. 2 shows the increased complexity of phase formation on the surface of alloy powder particles promotes the acceleration of aluminum matrix oxidation.

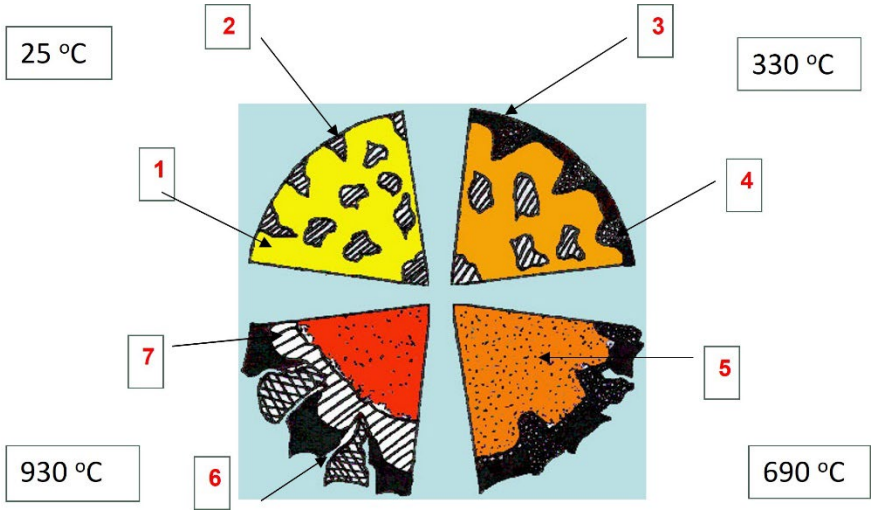

Fig.2. Structure of the particle and the oxide film on its surface changing during heating: 1) solid solution; 2) intermetallide; 3) Al_2O_3; 4) Al_2O_3, R_2O_3, $RAlO_3$; 5) melt; 6) $RAlO_3$; 7) Al_2O_3.(R - rare-earth element)

The achievement of these results required decades of work to analyse the concentration of alloying elements on particle surfaces using Auger electron spectroscopy (AES) and X-ray photoelectron spectroscopy (XPS), chemical and X-ray phase analysis of interaction products after heating to various temperatures, electron microscopy, and monitoring changes in the specific surface area of the powders.

Another method for modifying dispersed aluminum provides influencing the properties of the interaction products on the surface of oxidising Al particles. It involves the use of transition metal oxides. The study [12] demonstrates their positive role in the occurrence of thermite interaction with aluminum and the ability to deliver oxygen directly to the reaction zone on the surface of the oxidising particles. However, using mixtures of Al powders with oxide powders in the manufacturing process of energetic systems leads to a loss of direct contact between the particles. Consequently, methods ensuring the deposition of oxidisers directly onto the particle surface were developed [13, 14].

The development of *in situ* methods for studying heterogeneous reactions during heating in gas atmospheres has significantly accelerated the acquisition of information on the processes of the dynamics of phase formation and the kinetics of oxidation of metals and alloys. At the Institute of Nuclear Physics of the Siberian Branch of the Russian Academy of Sciences (SB RAS), in collaboration with researchers from the Institute of Solid State Chemistry and Mechanochemistry (Novosibirsk, Russia), phase formation processes occurring directly during programmed heating in gas atmospheres have been implemented at a synchrotron radiation source.

This paper reviewed the results of studying the oxidation of aluminum powders, its alloys with Ca and Ba produced by melt atomisation, dispersed Al with surfaces modified by transition

metal compounds in the form of corresponding gels deposited onto the particles. Using TG, DSC, and synchrotron X-ray phase analysis during programmed heating on air atmosphere, data on the dynamics of phase formation and the reasons of the physicochemical interaction processes occurring within the bulk and on the surface of the particles were obtained. The effectiveness of the experimental methods used to justify the selection of pathways for activating the oxidation of aluminum-based metallic fuels is assessed.

The purpose of this study is to evaluate the potential of using experimental methods providing information on the reactivity and dynamics of phase formation during the oxidation and combustion processes of metallic fuels.

Experimental Methodology and Materials

TG/DSC analysis of pure and alloyed Al was performed on a NETZSCH STA 449 F3 Jupiter thermal analyser using thin-walled alumina crucibles with an initial sample mass of approximately 15 mg. Heating was conducted from 25 to 1200 °C at a rate of 10 °C/min. The measurement cell with the sample was purged with an air flow (20% O_2 + 80% N_2) at a rate of 50 ml/min.

The morphology of the alloyed aluminum particles was studied using a TESCAN VEGA Compact LMH (s5121) and a JEOL JSM-6390LA analytical scanning electron microscope equipped with an energy-dispersive X-ray analyser (EDX). Chemical (elemental) analysis for the content of the modifiers used was performed by atomic emission spectrometry on a JY-48 inductively coupled plasma (ICP) spectrometer. The specific surface area of the powders was evaluated by low-temperature nitrogen desorption (BET method) on a TriStar 3000 automatic analyser (Micromeritics, USA). Particle size and size distribution were determined by laser granulometry on a Horiba LA-950 laser analyzer (Horiba, Japan).

Studies of phase formation features were conducted using a synchrotron radiation (SR) source at the "High-Pressure Diffractometry" and "Precision Diffractometry" stations installed on the fourth and sixth SR beamlines of the VEPP-3 electron storage ring (Shared Research Center "SSTRC", BINP SB RAS) [15, 16]. For high-temperature studies, an XRK-900 reactor chamber (Anton Paar, Austria) was used. The gas mixture was supplied using SmartTrak 50 gas flow controllers (Sierra, USA); reaction products were monitored by a quadrupole mass spectrometer (SRS UGA100, USA). The sample (volume ~0.15 cm^3) was heated at a rate of 10 °C/min, with a gas mixture flow rate of 50 ml/min. Phase analysis was performed using the ICDD PDF-2 powder database [17]. Quantitative phase analysis and refinement of crystal lattice parameters were conducted by the Rietveld method using the MAUD program [18].

Main body

Synthesis of Al-Ca, Ba alloys and powders based on them

There are many widespread methods of metalworking, i.e. reduction of metal oxides, hydrometallurgical and carbonyl processes, electrolysis of aqueous solutions and molten salts, and mechanical milling. However, melt atomisation is more advantageous industrial approach due to its relatively low energy consumption, high productivity and process efficiency, broad automation capabilities, and environmental cleanliness [17]. Atomisation is particularly

effective for producing multicomponent alloy powders, as it ensures volumetric uniformity of chemical composition and optimal particle shape. It is achieved by superheating the melt prior to atomisation resulted in a high degree of homogeneity at the atomic level due to the complete destruction of the solid-state hereditary structure, intense mixing, and rapid particle crystallisation with high cooling rates (ranging from 10-10^2 to 10^5-10^6 °C/s). Adjusting the cooling rate over a wide range allows ones to control over the microstructure, enabling the production of particles with varying grain sizes, free from defects such as inhomogeneous distribution of alloying components, and precise management of particle size [18].

The shape of atomised powder particles can be modified from perfectly spherical to highly irregular by regulating the process temperature between liquid metal disintegration and droplet solidification [19]. These factors collectively establish melt atomisation as the most promising method for producing high-quality metallic powders. When powder oxidation is unacceptable or high density and spherical particle morphology are required, atomisation with neutral or inert gases (nitrogen or argon) is applyed, eliminating the need for subsequent reduction annealing [20].

The powders of aluminum alloys with Ca, Ba, and the initial Al were produced using the UR-16-300-0.6-U4 installation manufactured by OOO Raspylitelnye Sistemy i Tekhnologii (Spray Systems and Technologies LLC) (Sverdlovsk region, Novouralsk, Russia). Fig. 3 shows the schematic diagram.

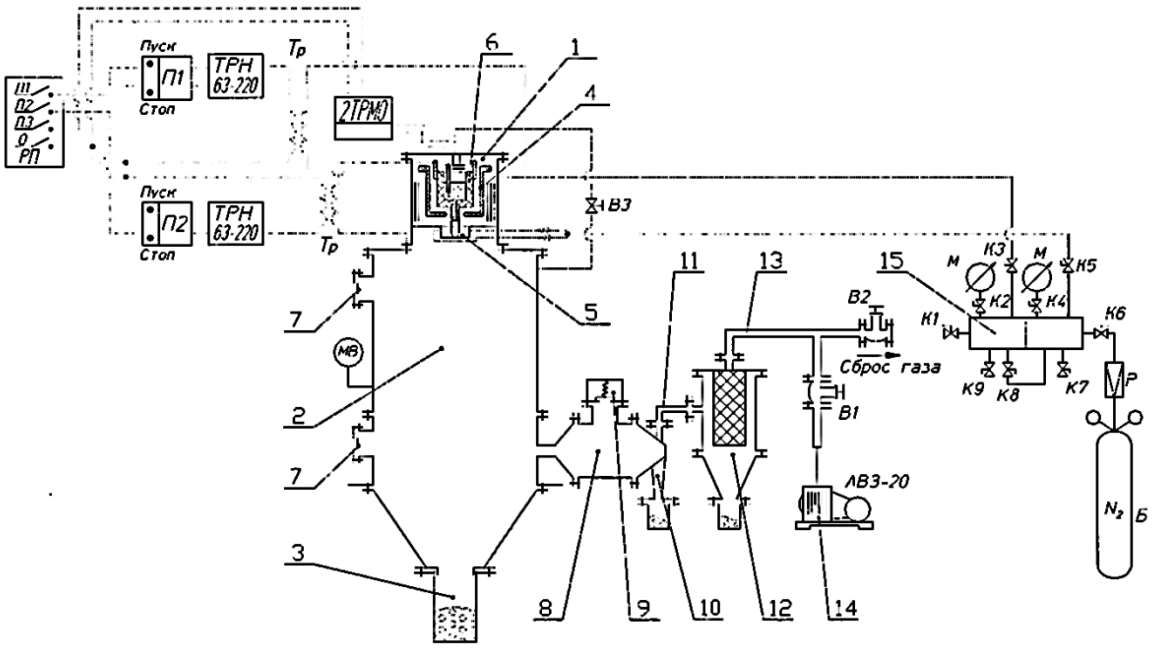

Fig.3. Schematic diagram of the installation for producing aluminum alloy powder by melt atomisation with nitrogen: 1) Melting furnace; 2) Atomisation chamber; 3) Powder collector; 4) Heater; 5) Atomisation nozzle; 6) Crucible; 7) Viewing window; 8) Cyclone; 9) Safety valve; 10) Cyclone collector; 11) Metal conduit; 12) Filter; 13) Turbo blower; 14) Fore-vacuum pump; 15) Gas manifold; Thyristor voltage regulator (TRN 1.2) for controlling the power of the furnace and metal conduit heaters.

The temperature regimes for atomisation were based on the phase diagrams of Al-Ca and Al-Ba presented in the following section. Alloying was conducted using master alloys composed of intermetallic compounds with the highest aluminum content. Before introducing them into molten aluminum, the intermetallics were ground to a particle size of no more than several tens

of micrometers. Grinding brittle intermetallic compounds reduces the melt homogenisation time prior to atomisation and lowers the required superheating temperature relative to the melting point of aluminum.

Ca and Ba and phase diagrams of binary systems based on aluminum

To accelerate the oxidation process of aluminum-based powders, the alloying element introduced into the Al melt must possess high oxidation capability and surface activity relative to aluminum in the liquid state. Calcium (Ca) and barium (Ba) were selected as such elements. Calcium demonstrates high chemical reactivity towards oxygen. On air, it oxidises more slowly than alkali metals because the oxide film formed on its surface is less permeable to oxygen. When heated, calcium burns with the release of a very large amount of heat [21]:

$$2Ca + O_2 = 2CaO + 635.5\ kJ/mol \quad (1)$$

The surface tension of calcium is 361 mJ/m^2 [10]. It is close or even lower to that of the most surface-active rare-earth elements – europium and ytterbium [10].

On the Al-Ca phase diagrams (Fig. 4), in the aluminum-rich region, there are intermetallic compounds characteristic of rare-earth elements. For instance, Al_4Ca forms through a peritectic reaction at 700 °C. However, the congruently melting intermetallic compound Al_2Ca melts at 1080 °C [22]. The aluminum-rich eutectic is identified at a temperature of 615 °C and a composition of 5.3 at.% Ca, with the solubility of Ca at this temperature being ~0.4 at.%.

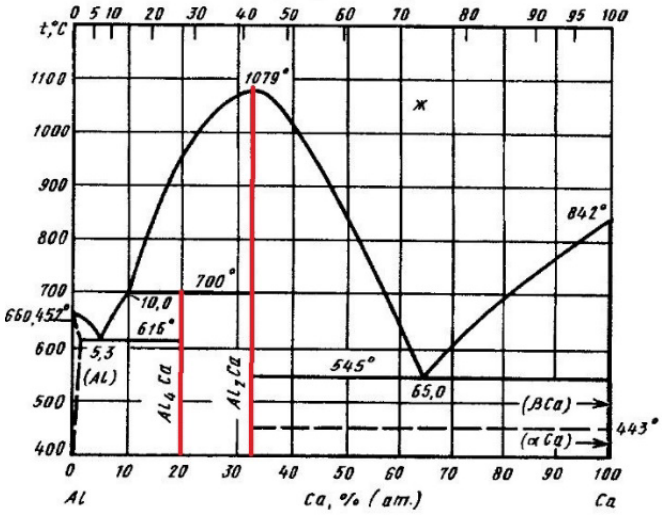

Fig.4. Al-Ca phase diagram.

Barium is chemically more reactive than calcium. Metallic barium is stored in sealed containers under petroleum or paraffin oil. On air, metallic barium loses its luster and becomes covered with a brownish-yellow film of oxide and nitride later turns gray:

$$Ba + ½\ O_2 = BaO + 556{,}9\ kJ/mol, \quad (2)$$

$$3Ba + N_2 = Ba_3N_2 + 376{,}1\ kJ/mol. \quad (3)$$

Metallic barium is used for the metallothermic reduction of most metals, including aluminum [23].

On the Al-Ba phase diagram [22], as in Al-rare earth metal (REM) systems, there are three compounds. The most aluminum-rich is Al_4Ba. It melts congruently at a temperature of 1105 °C (Fig. 5).

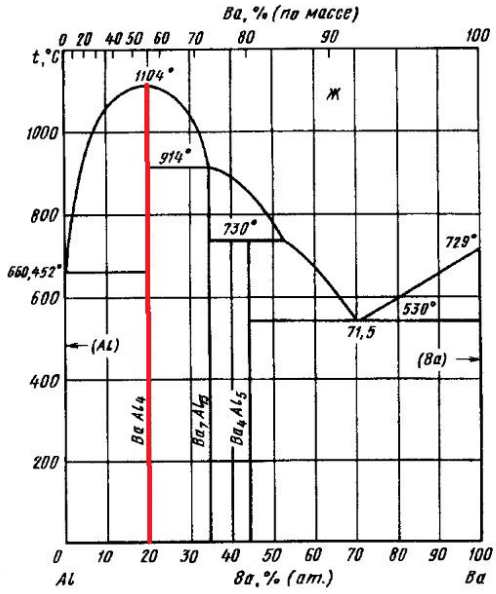

Fig. 5. Al-Ba phase diagram.

According to previous study [24], intermetallic compounds presented in the structure of aluminum-based alloys play a leading role in the oxidation process of powders, as they exhibit higher reactivity toward atmospheric oxygen than aluminum. When the alloys transit to the liquid state, the surface of the metallic core becomes enriched with the surface-active additive. They exist in the form of ordered microgroups corresponding to the most stable intermetallic compound [25]. Based on the results of study [26], the particle surface will be enriched with Ba due to the concentration of intermetallic groupings of the composition Al_4Ba in the Al-Ba system. A similar trend is expected for the Al-Ca system concentrating intermetallic groupings of Al_4Ca and Al_2Ca on the particle surfaces.

Figure 6 shows microimages of powders of aluminum alloys with Ca and Ba. Both powders have a nearly spherical shape.

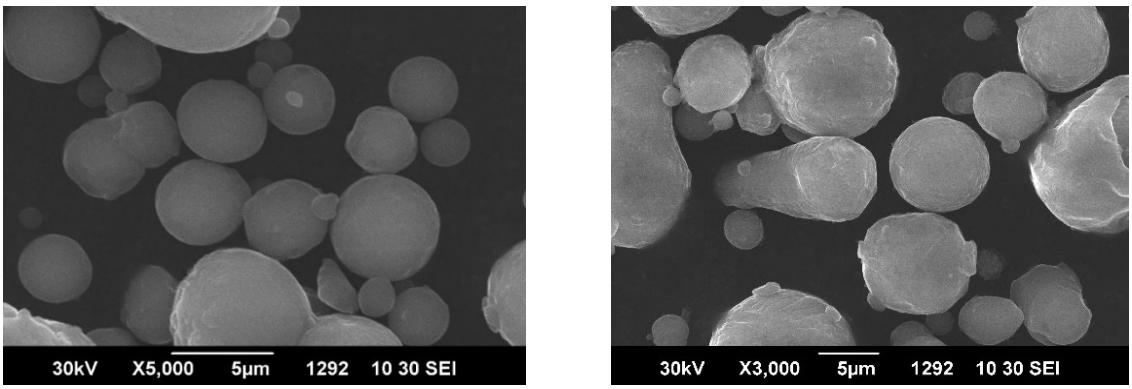

a) b)

Fig. 6. Microphotograph of Al-Ca (a) and Al-Ba (b) alloy powders.

According to chemical analysis, Ca content in the powder is about 0.88 at.%, and Ba is 0.26 at.%. According to XPS data [27, 28], Ca concentration on the surface is 34 at.%. Particles

of Ba alloy powder contain ~13 at.%. The specific surface area of the powder containing Ca is 0.2 m^2/g, and that of the alloy with Ba is 0.47 m^2/g. The average particle size is 11 μm and 5 μm, respectively.

Thus, aluminum-based powders containing reactive and surface-active metals (Ca and Ba) in an amount of 1.3 wt.% were obtained in accordance with the amount of master alloy introduced into the Al melt before powder production.

Methods for producing oxidation modifiers for aluminum-based powders and their application techniques to particle surfaces

To ensure close contact of modifiers with aluminum particle surfaces to enhance reactivity, methods for producing transition metal oxide compounds were developed. These were applied in the form of gels, penetrating the natural surface topography formed during melt atomisation crystallisation. After thorough mixing and appropriate thermal treatment, a composite powder with an additional shell of transition metal oxide was formed. Below there are examples of two developed methods for modifying Al with V_2O_5 and Fe_2O_3.

Modification with V_2O_5

The method is based on the thermolysis of V_2O_5 by pouring its melt into intensely stirred distilled water. In this case, a $V_2O_5 \cdot nH_2O$ hydrogel forms instantly upon contact of the melt with cold water. Almost all vanadium in the gel is in the pentavalent state. The vanadium content in the gel can be regulated by evaporation, up to a paste or even solid state, i.e., forming xerogels with minimal water content and a unique structure [13, 29]. The gel can be applied using vacuum filtration or, in the case of a paste state, by mixing the components.

According to scanning electron microscopy, impregnation with V_2O_5 gel does not change the shape of the original Al powder particles (Fig. 7). Adsorption measurements showed an increase in specific surface area. Moreover, Hall funnel flow tests indicated a significant improvement in flowability [29].

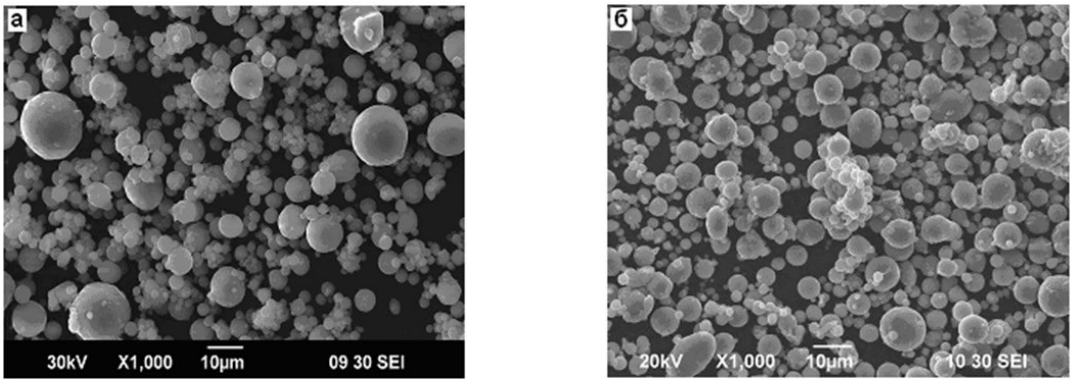

Fig.7. Morphology of Al particles: a) initial; b) modified with $V_2O_5 \cdot nH_2O$.

Modification with iron formate

Modification was conducted according to a patented method [30] by mixing the metal powder with a gel of basic iron(II) formate – $Fe(OH)(HCOO)_2$. To obtain the gel, a method based on the interaction of iron nitrate ($Fe(NO_3)_3 \cdot 9H_2O$) with diluted formic acid under mild

heating was used. The solution was held at 80 °C until the release of gaseous products ceased and then evaporated at the same temperature to form a bulk orange precipitate of basic iron formate. The precipitate was separated from the mother liquor by vacuum filtration and air-dried at 50 °C for 1 hour. To prepare the modified aluminum powder, the required amount of $Fe(OH)(HCOO)_2$ was dissolved in distilled water at 80 °C and cooled to room temperature. It was then mixed with Al powder in a porcelain cup. To remove water and decompose the iron formate, the sample was dried at 100 °C for 0.5 hours and then calcined at 350 °C for 1 h. The calcination temperature was selected based on thermal analysis data. Those indicate that the decomposition of $Fe(OH)(HCOO)_2$ during heating in air occurs exothermically in a single stage.

After modifying the surface of the aluminum powder with iron oxide in an amount of 2 wt.% (in terms of metal), the particle surface becomes rougher (Fig. 8).

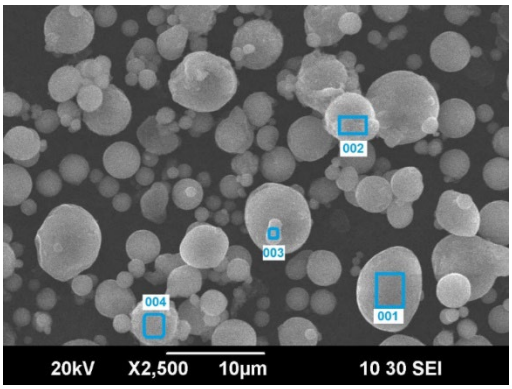

Fig.8. Electron micrograph of Al powder particles modified with Fe_2O_3.

Local analysis by energy-dispersive X-ray spectroscopy (EDX) confirms the presence of Fe_2O_3 on the particle surface; the Fe content in the sample is close to the calculated value.

Results of the oxidation study of aluminum-based powders using TG and DSC methods

Figure 9 shows the results of the oxidation study of aluminum powder produced by melt atomization [27].

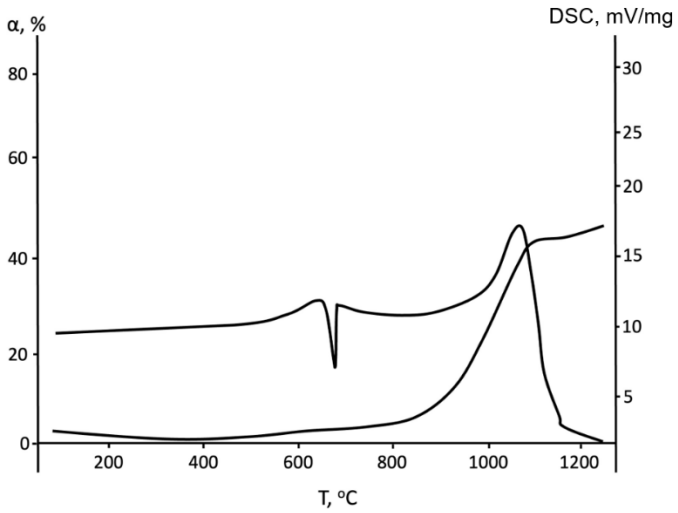

Fig. 9. TG and DSC curves of initial aluminum.

At the initial stage of interaction (550-700 °C), an exothermic effect is observed. It is associated with the disruption of the protective properties of aluminum oxide on the particle surface due to the transition of amorphous Al_2O_3 to the crystalline γ-form, and an endothermic effect of melting of the Al sample. Above the melting point, under the studied heating regimes, a single maximum appears on the DSC curve at a temperature of about 1060 °C. The specific heat released as a result of oxidation is 1840 J/g; the completeness of oxidation is about 41%.

For the Al-Ca alloy (Fig. 10), a more complex heat release pattern is characteristic in the active oxidation region [27].

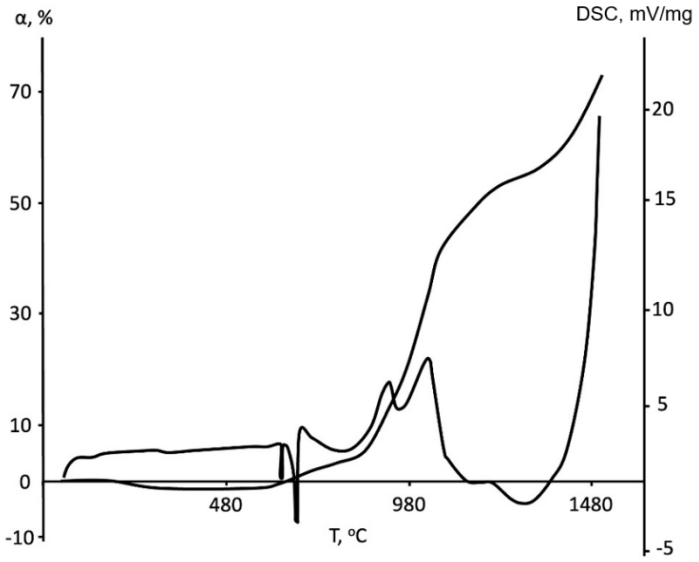

Fig.10. TG and DSC curves of Al-Ca alloy.

Two maxima are observed on the DSC curve: the first at approximately 920 °C and the second at about 1030 °C. The specific heat released is 2104 J/g; including the heat in the region of the first maximum it is 686 J/g. It practically coincides with the melting temperature of the alloy. The degree of conversion is about 73%, indicating an increase in oxidation activity.

For the Al-Ba alloy powder [28], oxidation accelerates immediately after melting. An exothermic effect is recorded on the DSC curve with an area corresponding to 265 J/g (Fig. 11).

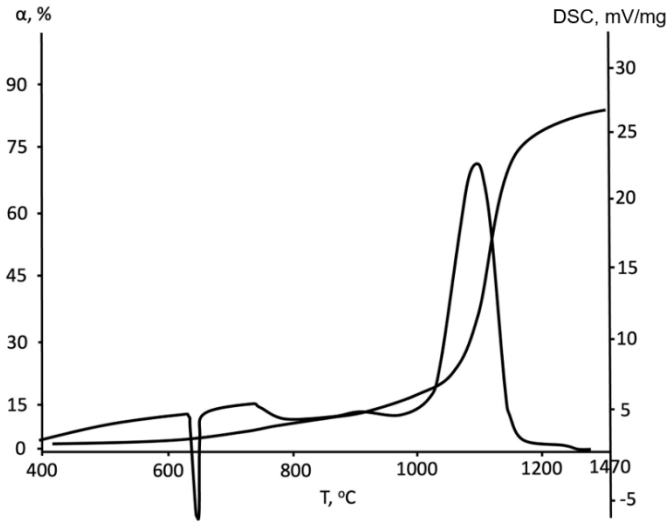

Fig.11. TG and DSC curves of Al-Ba alloy.

It is followed by a second acceleration region of oxidation with a maximum heat release at 1110 °C. The specific heat release increases to 9026 J/g. The total heat release during heating of the sample to the maximum temperature is more than 8 times higher than that of the pure (initial) aluminum powder. The degree of conversion is about 85%.

Figure 12 shows the TG and DSC curves of Al powder modified by applying a V_2O_5-based gel to its surface. For ease of comparison of the obtained powder, data for the initial aluminum without modification are presented. The oxidation process of the powder begins at temperatures around 500 °C. It is below the melting points of Al (660 °C) and V_2O_5 (678 °C). The DSC curve at a metallic vanadium concentration of 0.78 wt.% shows an exothermic effect with a maximum at 800 °C. It is 250 °C lower than that of the initial aluminum powder. The degree of conversion at 1000 °C is over 80%. Indeed, the unmodified aluminum powder at this temperature is only approximately 20% oxidised.

In terms of reactivity during heating in air, the presented composition is not inferior to and even surpasses the Alex powder obtained by the explosion of aluminum wire. The degree of conversion of Alex powder at 1000 °C is 69% [8].

Along with assessing the reactivity of the developed modified metallic fuel powders, thermogravimetry and scanning calorimetry data provide optimising the search for new modifiers and the conditions for their application to powder surfaces. The use of additives [31-33] of oxides such as WO_3, MoO_3, V_2O_5, Ta_2O_5, I_2O_5, TiO_2, Cr_2O_3, Fe_2O_3, Bi_2O_3, CuO (strong oxidisers and direct surface reactions along the thermite type) activates aluminum combustion. However, practical interest to the modifiers that can be combined with metal powders in a gel state, ensuring close contact with their surface. It is important in the process of obtaining composite formulations for energetic systems.

Therefore, a search for modifiers from the series of formates of manganese, iron, cobalt, and nickel was conducted, their synthesis was performed, and their effect on the reactivity of aluminum powder was studied [34]. The formates were analysed on a thermal analyser when heated to 400 °C in an air environment. Figure 13 shows the TG and DSC curves of Mn, Fe, Co, and Ni formates. The obtained results were used to select the conditions for forming coatings on the surface of aluminum powders.

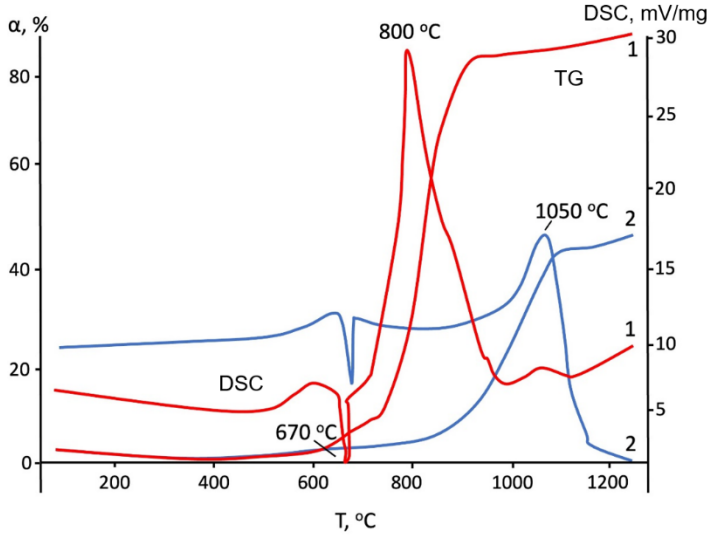

Fig.12. TG and DSC curves: 1 – Al modified with $V_2O_5 \cdot nH_2O$ gel at a vanadium concentration of 0.78 wt.%; 2 – initial aluminum.

Depending on the temperature regimes and gas environment of modifying, an oxide or metallic coating can be formed on the particle surfaces.

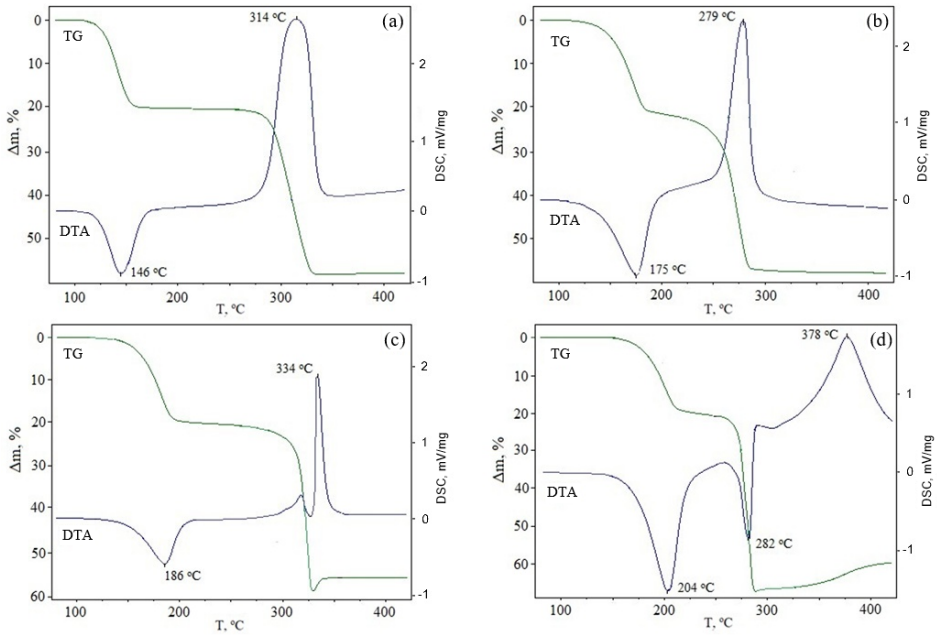

Fig.13. TG and DSC curves of $M(HCOO)_2 \cdot 2H_2O$; M = Mn (a), Fe (b), Co (c), Ni (d).

Fig. 14 shows the TG and DSC curves of samples of spherical dispersed aluminum powder (ASD-4) modified by impregnation with solutions of $M(HCOO)_2 \cdot 2H_2O$, where M = Mn, Fe, Co, Ni, at a dosage of 2 wt.% in terms of metal content.

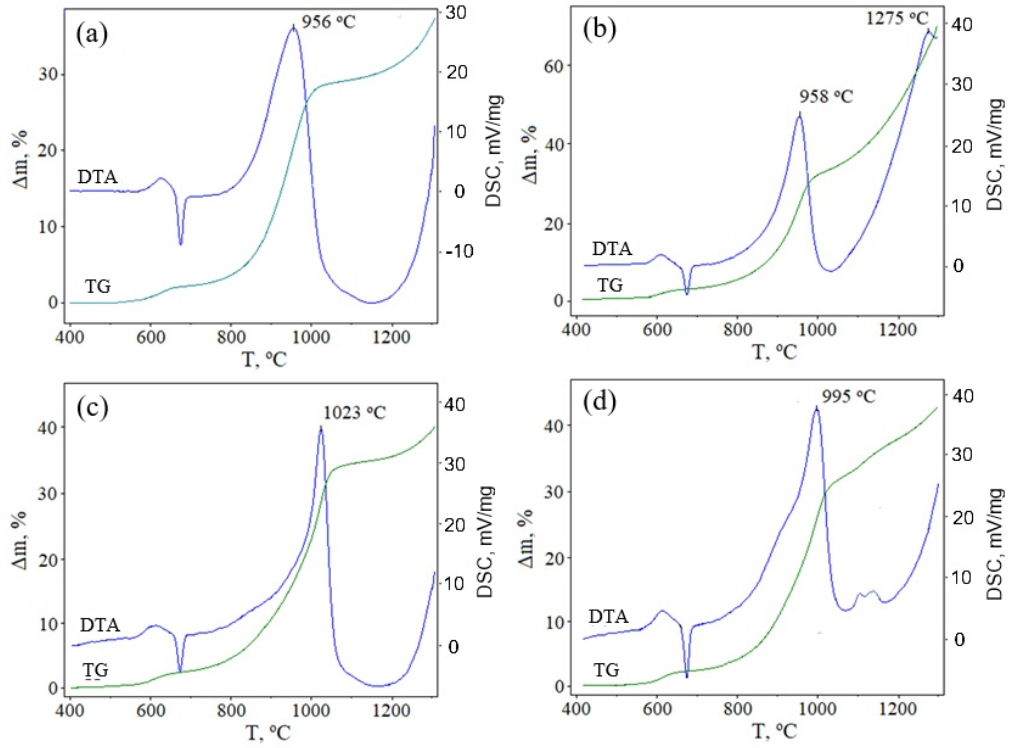

Fig.14. TG and DSC curves of ASD-4 powder samples modified by impregnation with solutions of $M(HCOO)_2 \cdot 2H_2O$, where M = Mn (a), Fe (b), Co (c), Ni (d), after heating on air at 350 °C for 30 minutes.

According to Fig. 14, a noticeable increase in the degree of oxidation occurs only when modified with iron formate.

Based on the examples, the developed modifiers significantly enhance the reactivity of aluminum-based powders.

Results of X-ray phase analysis using a synchrotron radiation source

Aluminum powder

Information on the phase composition of a sample heated directly in the focus of the radiation beam allows ones to analyse the interaction of Al in a single experiment. It is comprehensively presented in Fig. 15. showing diffraction patterns of ASD-4 powder at various heating temperatures above the melting point of aluminum.

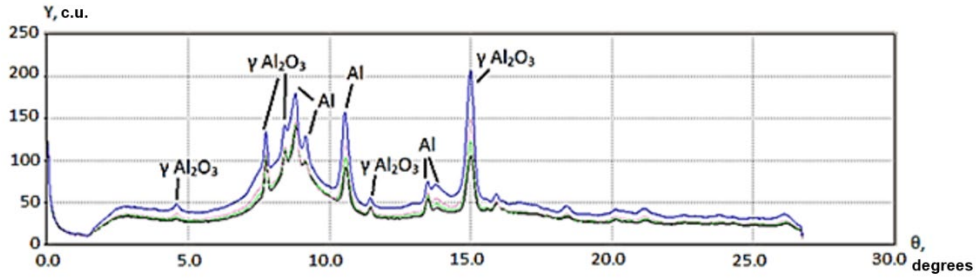

Fig.15. Diffraction pattern of ASD-4 powder at temperatures: black line is 700 °C; green is 800 °C; blue is 900 °C.

Against the background halo of the liquid phase, clear lines of oxide phases formed during oxidation are recorded on the diffraction spectra. Their intensity increases with rising temperature. However, at the time of obtaining this information, the method's capabilities were limited to measurements with steps of several tens of degrees. Nevertheless, the high sensitivity of the detector provides the detection of small amounts of the resulting interaction products.

Aluminum modified with Ca

Based on the results of diffraction studies (Fig. 16) using synchrotron radiation (SR), the initial sample consists of three phases: a solid solution of calcium in aluminum, the intermetallic compound Al_4Ca, and a small amount of Al_2Ca. This pattern persists up to the melting point, with only peak shifts occurring due to increased lattice parameters caused by thermal expansion.

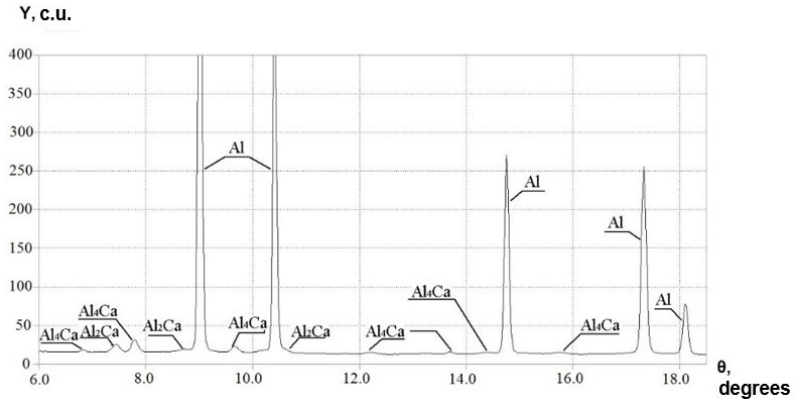

Fig.16. Diffraction pattern of Al-Ca powder at 500 °C.

After melting, the peaks from aluminum and intermetallic compounds disappear, and peaks from phases of corundum, grossite ($CaAl_4O_7$), and chi-Al_2O_3 occur against the background of scattering from the liquid alloy (Fig. 17).

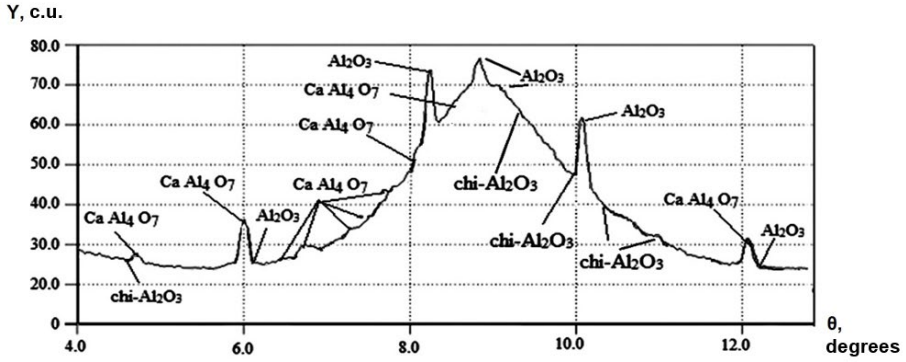

Fig.17. Diffraction pattern of Al-Ca powder heated to 750 °C.

Upon further heating, up to the maximum temperature, there are phases of corundum, grossite, and chi-Al_2O_3. The liquid phase persists when heated to 1000 °C. As the temperature raises, the quantity and intensity of lines from aluminum oxide and grossite ($CaAl_4O_7$) significantly increase (Fig. 18).

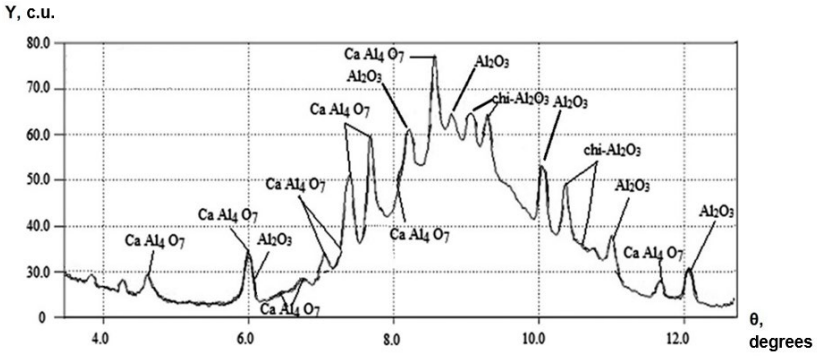

Fig.18. Diffraction pattern of Al-Ca powder heated to 1000 °C.

Figure 19 shows the results of the thermal analysis of powders: Al-Ca alloy (1) compared to the initial aluminum (2).

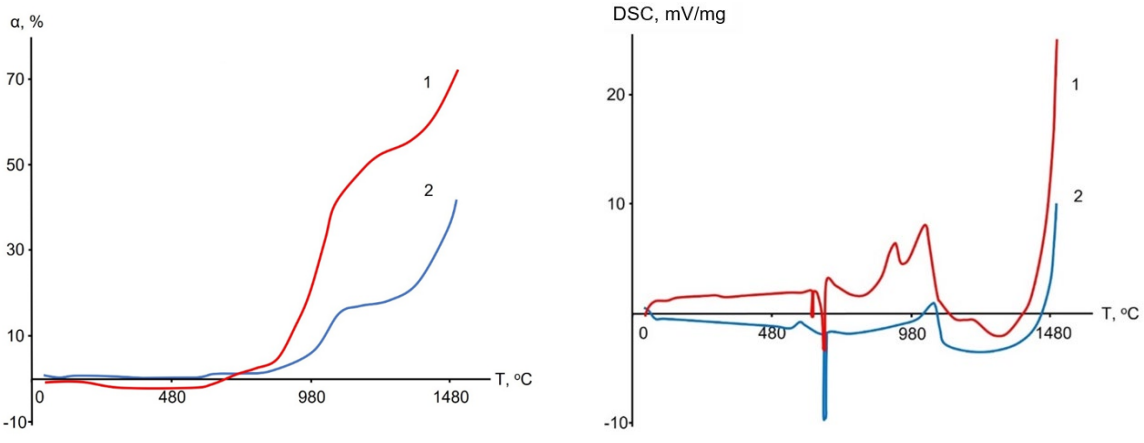

(a) (b)

Fig.19. TG (a) and DSC (b) curves: 1) aluminum-calcium alloy; 2) pure aluminum.

According to Fig. 19, at the temperature range of 1025–1280 °C the degree of conversion of the calcium-alloyed powder is two or more times higher than that of pure aluminum. Moreover, at the maximum heating temperature of 1480 °C, the oxidation completeness of the alloy powder is 1.65 times higher.

By a comparison of the obtained results, the presence of three phases (two intermetallic compounds and aluminum) in the structure of the initial alloy particle significantly alters the thermokinetic patterns of aluminum oxidation. Starting from 730 °C, the oxidation process intensifies sharply. In addition to aluminum oxide, grossite ($CaAl_4O_7$) is formed, resulting from the interaction of calcium and aluminum oxides.

Thus, alloying aluminum with calcium significantly enhances the oxidation completeness of aluminum-based powder. Indeed, calcium exhibits high surface activity toward aluminum and high reactivity with oxygen, This is particularly evident in the initial stages of interaction, at temperatures up to ~1280 °C. Apparently, within this temperature range, the main mass of the alloying additive determining the oxidation features is consumed due to the constant replenishment of the liquid alloy surface with calcium. As seen in Fig. 19, above 1280 °C the TG curves exhibit similar behavior. Such interaction character confirms the proposed mechanism of oxidation presented in the study [11].

Aluminum modified with Ba

Similar studies were conducted for the Al-Ba system. As shown by the diffraction results of the Al-Ba powder (Fig. 20a), the initial phase composition of the powder (Al, Al_4Ba, Al_2O_3) persists up to the melting point of the eutectic. A broad scattering maximum from the liquid phase appears on the diffraction pattern (Fig. 20b).

According to [22], the eutectic melts at a temperature of 651–652 °C. It is consistent with the observed heating temperature of 650 °C.

With subsequent temperature increase, during the analysis of the phase composition of oxidation products by X-ray diffraction, a growth in the intensities of maxima corresponding to the intermetallic compound Al_4Ba is observed (Fig. 20c). Upon further heating, it oxidises to form double oxides $BaAl_2O_4$ и $Ba_{0,83}Al_{11}O_{17,33}$ (Fig. 20d). The occurence of these phases in the oxidation product layer, along with γ and α forms of individual aluminum oxide, reduces the protective properties of the barrier layer, as they have different structures and physico-mechanical characteristics. It is confirmed by electron microscopy data of the initial powder and oxidation products (Fig. 21).

The oxidation products have a fragmented form of hollow oxide shells and smaller fragments. This phase formation pattern facilitating the access of atmospheric oxygen to the metallic surface. It is confirmed by the TG and DSC curves (Fig. 22).

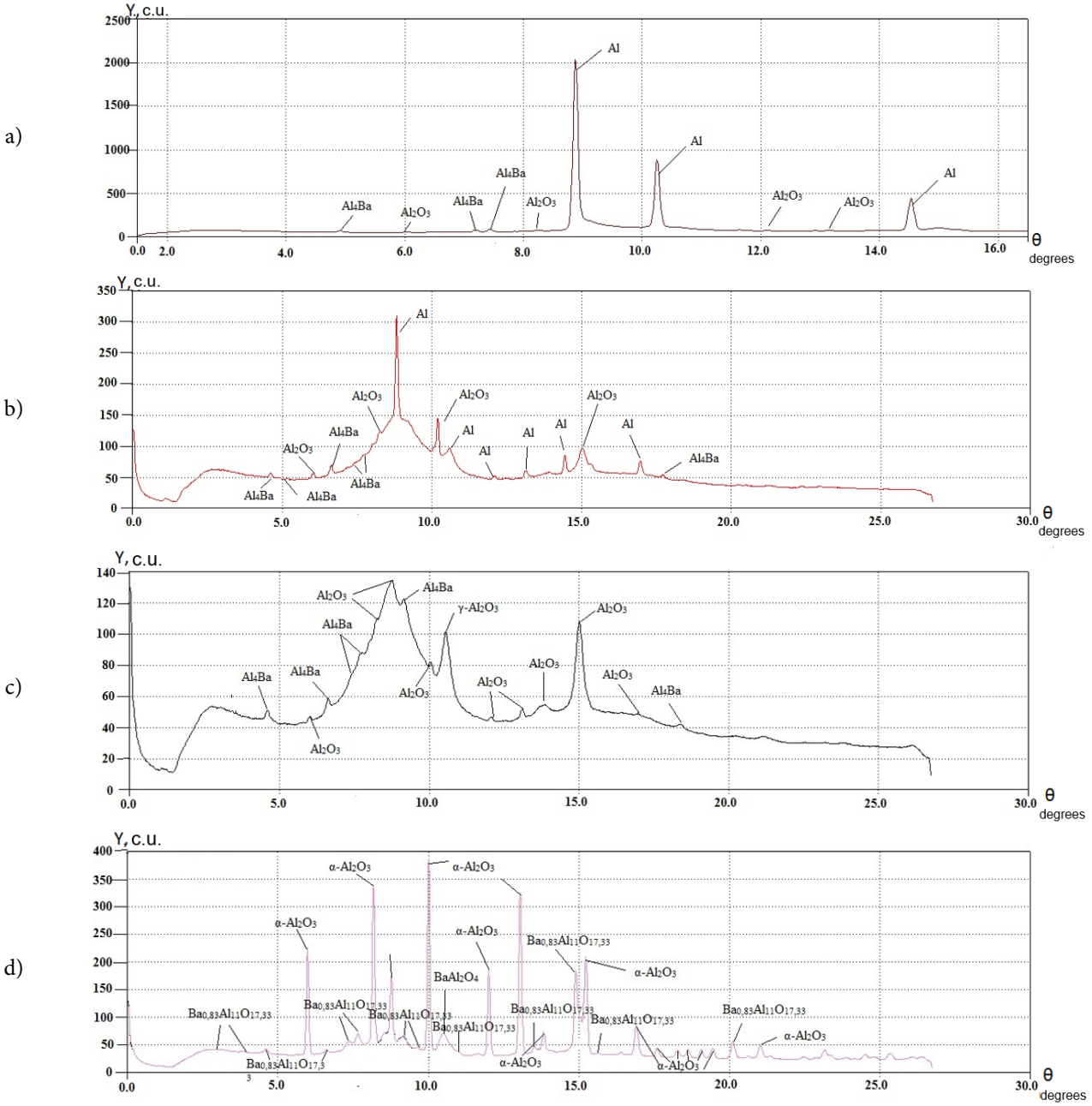

Fig.20. Diffraction patterns of the Al-Ba sample at: a) 500 °C; b) 650 °C; c) 750 °C; d) 1000 °C.

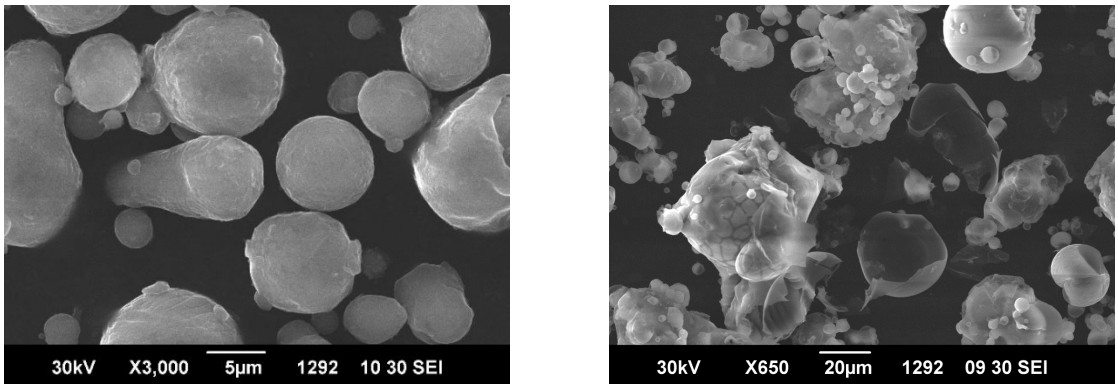

a) b)

Fig.21. Morphology of Al-Ba powder particles: a) initial; b) oxidised upon heating to 1000 °C.

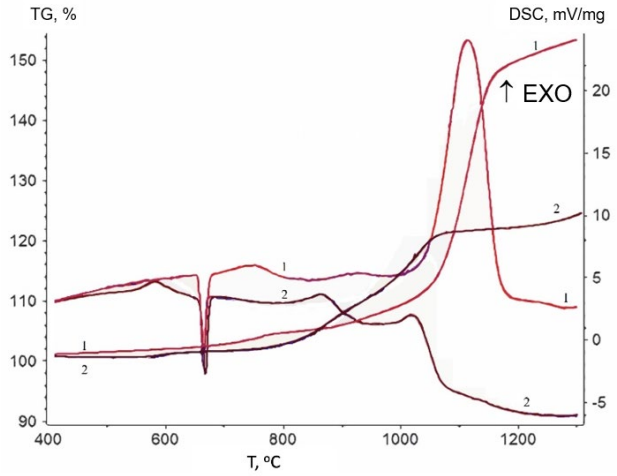

Fig.22. TG and DSC curves: 1) Al-Ba alloy (S_{sp}= 0.47 m^2/g); 2) Al (S_{sp} = 0.4 m^2/g).

According to thermograms comparison, up to the melting point the pure aluminum powder oxidises vigorously than the alloy itself. As previously established [35], it is due to the removal of diffusion limitations during the transition of amorphous aluminum oxide to the crystalline γ-form Al_2O_3 causing an exothermic effect with a specific heat release of 237 J/g. It is followed by endothermic effects of melting of aluminum and the alloy. Upon further heating, the alloy powder oxidises more efficiently. Immediately after melting, oxidation accelerates, and an exothermic effect is recorded on the DSC curve, with an area corresponding to 265.1 J/g. Then follows a second stage of oxidation acceleration, detected on the TG curve by a change in slope and the appearance of a new exothermic region, transitioning into a large exothermic peak with maximum heat release at 1110 °C. The specific heat release here is 9026 J/g. The total heat release during heating of the samples to the maximum temperature (1573 °C) for the alloy is 8.4 times higher than for the aluminum powder. The maximum mass gain during heating of the Al powder with a specific surface area of 0.4 m^2/g is 44% of that for the Al-Ba alloy powder.

Thus, the high surface and chemical activity of both Ca and Ba allow them to be recommended as effective additives modifying the characteristics of aluminum-based powders used as fuels in energetic condensed systems.

Aluminum modified with V_2O_5

Results of diffraction studies using synchrotron radiation (SR) during heating of a modified V_2O_5 ASD-4 powder sample to 650 °C showed the phase composition consists of Al, Al_2O_3 и V_2O_5 at the initial stage of the oxidation process (Fig. 23a). Above this temperature, i.e., after the transition of aluminum and the modifier V_2O_5 to the liquid state (Fig. 23b), lines of $AlVO_4$ occur on the diffraction spectra; the lines corresponding to all crystalline forms of metal oxides (Al_2O_3, V_2O_5) disappear. A further increase in temperature leads to the occurence on the diffraction pattern of intense maxima from aluminum oxide (α-Al_2O_3) and weak reflections due to the formation of intermetallic compounds of the compositions Al_3V и Al_8V_5 (Fig. 23c) presented on the phase diagram of the Al-V system [22]. On the diffraction patterns of samples taken at the maximum possible temperature of 1100 °C under experimental conditions, the intensity of lines of metallic phases noticeably decreases, and the halo from the liquid phase disappears (Fig. 23d). The obtained results are consistent with the data provided in [36] on the course of interaction processes in the thermite system based on metallic aluminum and V_2O_5.

a)

b)

c)

d)

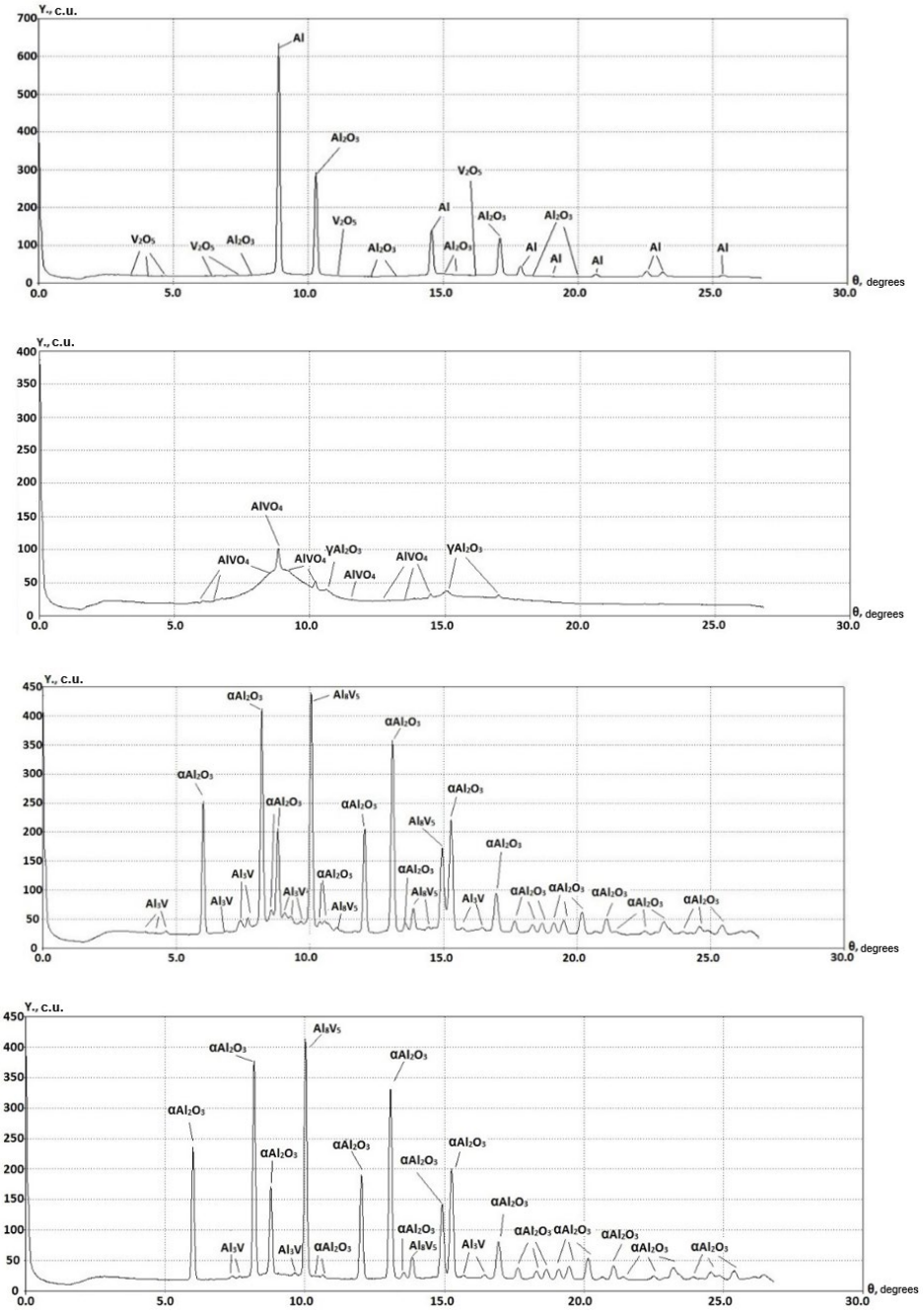

Fig.23. Diffraction patterns of aluminum modified with V_2O_5 at temperatures: a) 500 °C; b) 650 °C; c) 900 °C; d) 1100 °C.

Based on the analysis of the obtained experimental and literary data [37-39], the mechanism of the effect of V_2O_5 additives on the oxidation process of ASD-4 can be represented in the following sequence. Upon melting, liquid aluminum destroys the oxide shell and contacts with V_2O_5. At a temperature of about 680 °C it transits to the liquid state and interacts with aluminum oxide according to reaction (4), forming $AlVO_4$:

$$V_2O_5 + Al_2O_3 \rightarrow 2AlVO_4. \quad (4)$$

Simultaneously occurring intensive oxidation of aluminum, accompanied by an increase in sample temperature, leads to the melting of $AlVO_4$ [40]. The diversity of practically

simultaneous processes in the volume and on the surface of the sample is associated with the polyvalency of vanadium. It promotes efficient oxygen transfer to the reaction zone, resulting in intensive self-heating of the system.

According to [41], as a result of detailed diffraction analysis under conditions of small temperature interval measurements, the formation of $AlVO_4$ was observed. It was formed at a temperature of 600 °C (Fig. 24), close to the temperature of $AlVO_4$ formation (T=620 °C) estimated in [36] to study interaction of mixture components with a composition of 33% Al – 67% V_2O_5 using high-temperature X-ray phase analysis.

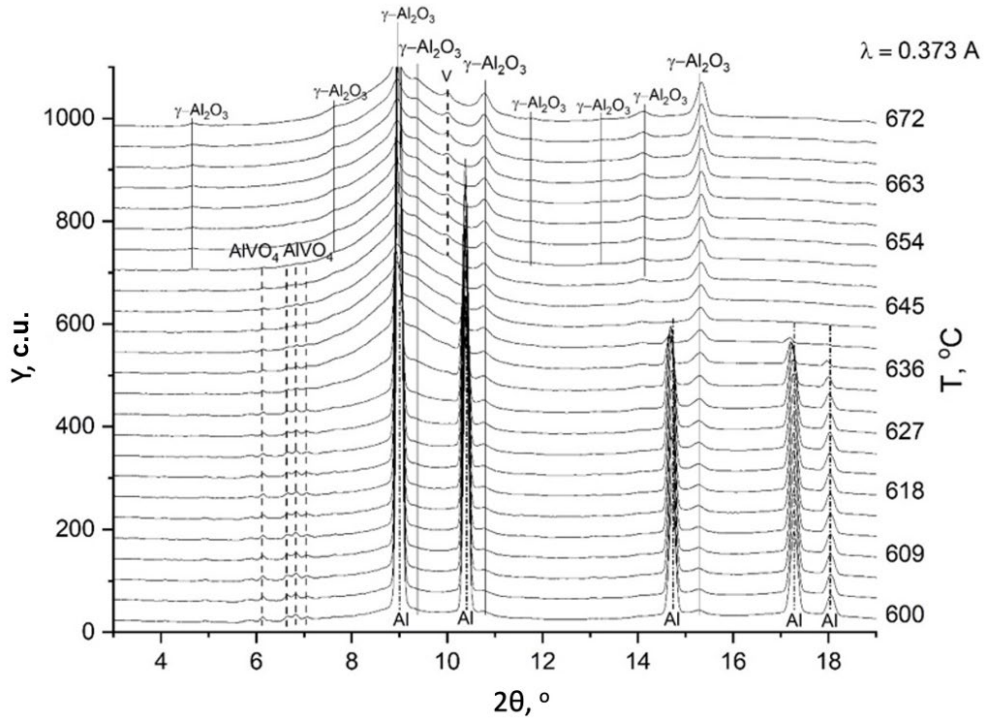

Fig.24. Series of diffraction patterns of the Al-V_2O_5 system at 600-672 °C.

Indeed, the temperatures of processes under conditions of intensive oxidation and combustion is a very complex issue relating with many biases. In [36], the relative bias in temperature determination was about 5%. The bias in our experiment is estimated within the same limits; the thermocouple in a corundum sheath was placed at a distance of 0.1-0.2 mm from the sample and the same distance below the radiation beam. Direct contact of the thermocouple with the reaction front in this diffraction method setup is very difficult to achieve. Real reduction in the onset temperature of interaction can also be caused by dimensional factors of the interacting particles [42, 43]. It can be assumed that nanoscale layers of V_2O_5 and γ-Al_2O_3, as established above by ellipsometry, can interact at lower temperatures [42, 43], initiating the oxidation process.

Upon further heating, γ-Al_2O_3 forms at about 642 °C, and reflections of crystalline aluminum disappear. It indicates the transition of the main mass of aluminum to the liquid state. It is 18 °C below the reference melting temperature and suggests an underestimation of the actual sample temperature by the thermocouple. After melting, the occurence of lines of metallic vanadium, the nucleation of α-Al_2O_3, and an increase in the intensity of γ-Al_2O_3 reflections are observed (Fig. 25).

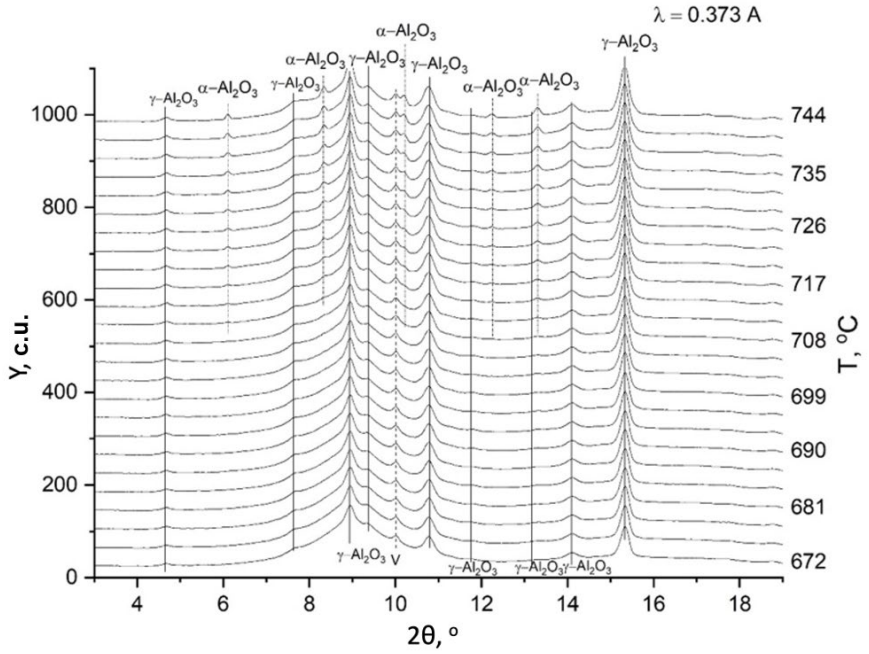

Fig.25. Series of diffraction patterns of the Al-V_2O_5 system at 672-744 °C.

Heating in the range of 744-798 °C indicates a significant increase in the amount of the high-temperature modification of oxide, α-Al_2O_3 (Fig. 26). The line of metallic vanadium persists, and only at the maximum experimental temperature (798 °C) is a reflection corresponding to VO observed in the interaction products.

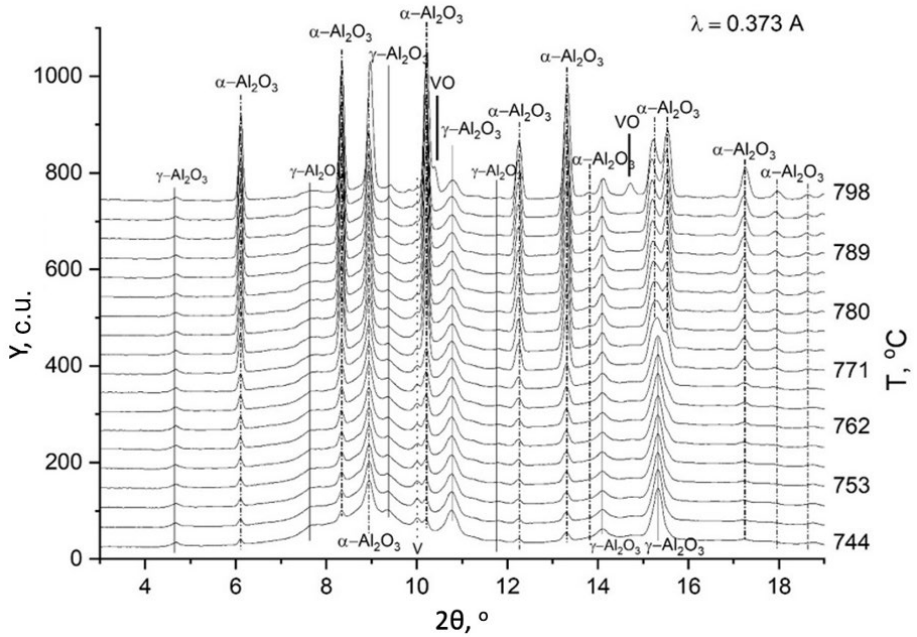

Fig.26. Series of diffraction patterns of the Al-V_2O_5 system at 744-798 °C.

To ensure the reliability of the obtained diffraction patterns, a full-profile analysis of the phase composition was performed using the Rietveld method with the MAUD (Materials Analysis Using Diffraction) software [44] and the COD (Crystallography Open Database) databases [45]. As an example, Fig. 27 shows the results of the analysis of the diffraction pattern obtained at 600 °C.

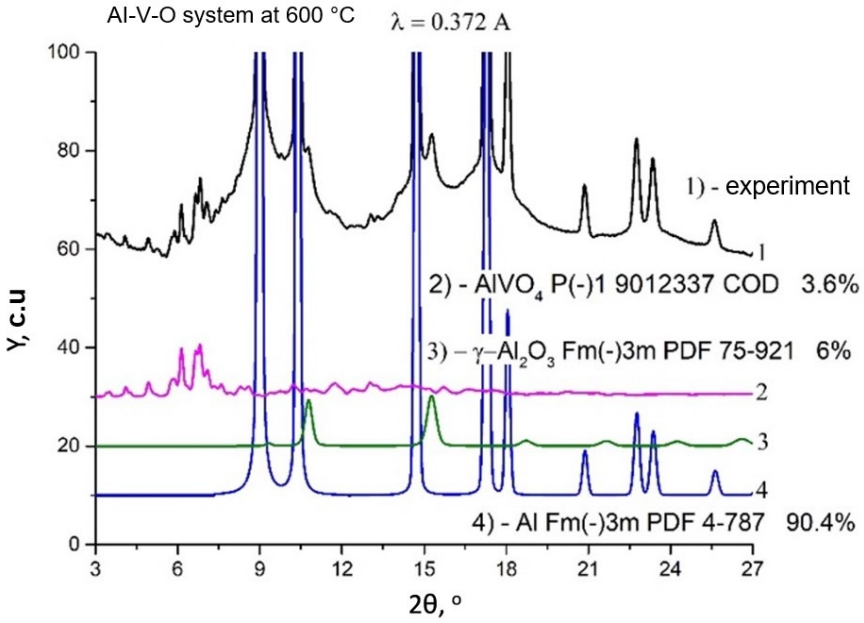

Fig.27. Diffraction pattern of ASD-4 modified with $V_2O_5 \cdot nH_2O$ at 600 °C.

According to Fig. 27, the content of $AlVO_4$ is about 3.6 wt.%; a content of liquid aluminum and γ-Al_2O_3 is approximately 6 wt.%. The results of full-profile analysis at temperatures of 672-772 °C indicate a content of metallic vanadium of about 0.8-0.9 wt.%. It agrees with the results of chemical analysis of vanadium in the modified layer (0.8 wt.%). However, it is impossible to identify phases containing vanadium at the temperature above 772 °C.

In addition to phase transitions in the oxide layer and metal, the oxidation process of ASD-4 modified with V_2O_5 is influenced by chemical reactions between the components of the Al-Al_2O_3-V_2O_5-O_2 system.

The thermite reaction and the reaction of formation of low-melting oxide $AlVO_4$ (4) initiate aluminum oxidation. Constant changes in the phase composition of oxidation products, associated with the surface activity of vanadium oxide and its polyvalency, cause disturbances. They lead to the loss of protective properties by the oxide film on the particle surface and facilitate heat and mass transfer to the chemical reaction zone.

Aluminum modified with $Fe(OH)(HCOO)_2$

To study the behavior of ASD-4 powders modified with gel during oxidation in air, samples containing 1, 5, and 10 wt.% Fe (in terms of metal) were prepared according to the developed methodology. According to synchrotron radiation X-ray diffraction data (Fig. 28), ASD-4 powders obtained by impregnation with gel and heating in air to 350 °C already contain, in addition to iron oxide in the form of γ-Fe_2O_3, the phase α-Fe_2O_3. The intensity of α-Fe_2O_3 reflections increases with the amount of modifier.

The observed phase formation pattern may be due to the specifics of thermolysis of the gel applied to the oxide surface of aluminum powder particles. According to [46], the phase transition γ-Fe_2O_3→α-Fe_2O_3 begins above 350 °C and completes at 550 °C. It is associated with the exothermic effect of the transformation of maghemite into hematite with a maximum on the DTA curve at 560 °C (Fig. 29).

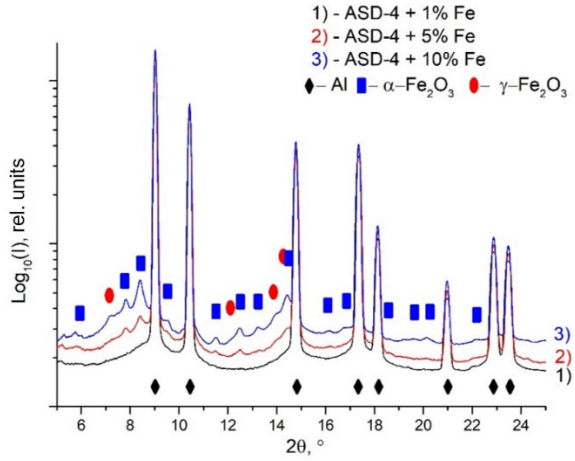

Fig.28. Diffraction patterns of modified aluminum powders with 1, 5, and 10 wt.% Fe content, obtained by impregnation with $Fe(OH)(HCOO)_2$ gel and heating on air to 350 °C.

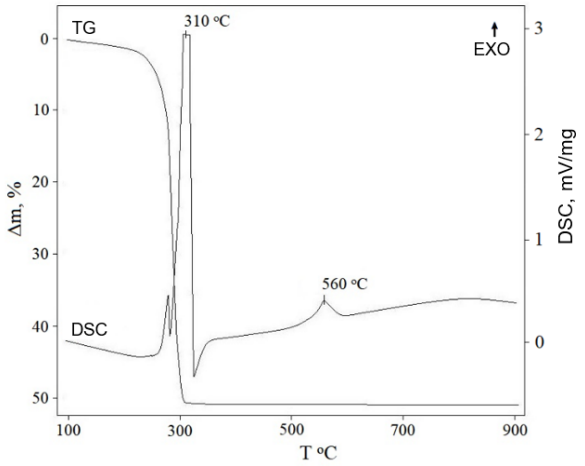

Fig.29. Results of thermal analysis of iron formate $Fe(OH)(HCOO)_2$ by TG and DSC methods.

Processes in the oxide shell on the surface of aluminum particles during heating, associated with the formation of γ-Al_2O_3, may also influence the phase transition of maghemite to hematite. They occur with the release of crystallisation heat from the amorphous phase of aluminum oxide in this temperature range.

Figure 30 shows diffraction patterns of modified ASD-4 powder with 10% Fe content, obtained directly during oxidation at heating in an air environment.

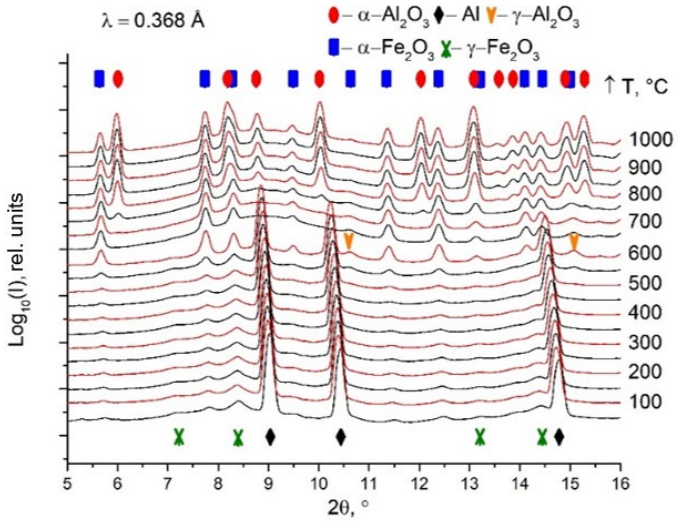

Fig.30. Diffraction patterns of modified aluminum powder with an iron content of 10 wt.%.

An increase in temperature to 500 °C does not lead to significant phase changes in the sample. At 550 °C, the reflections of γ-Fe_2O_3 disappear, and the reflections of α-Fe_2O_3 become more intense. After the transition of aluminum to the liquid state at about 660 °C, an increase in the concentration of aluminum oxide in the form of α-Al_2O_3 is observed. It becomes intense at temperatures above 750 °C. During the oxidation process, iron stabilises as α-Fe_2O_3, upon further temperature increase up to 1000 °C. However, no iron-containing phases are formed, such as Fe, Fe_3O_4, FeO, Fe_3Al, AlFe, $FeAl_2O_4$ observed as intermediate products in the interaction of components in the Al – Fe_2O_3 thermite system [47-49].

Figure 31 shows visually the temperature dependencies of the phase quantities formed during the oxidation of the ASD-4 + 10% Fe sample. Each set of points by temperature corresponds to one diffraction pattern from Fig. 30. Accordingly, the phases have different weight contributions during heating.

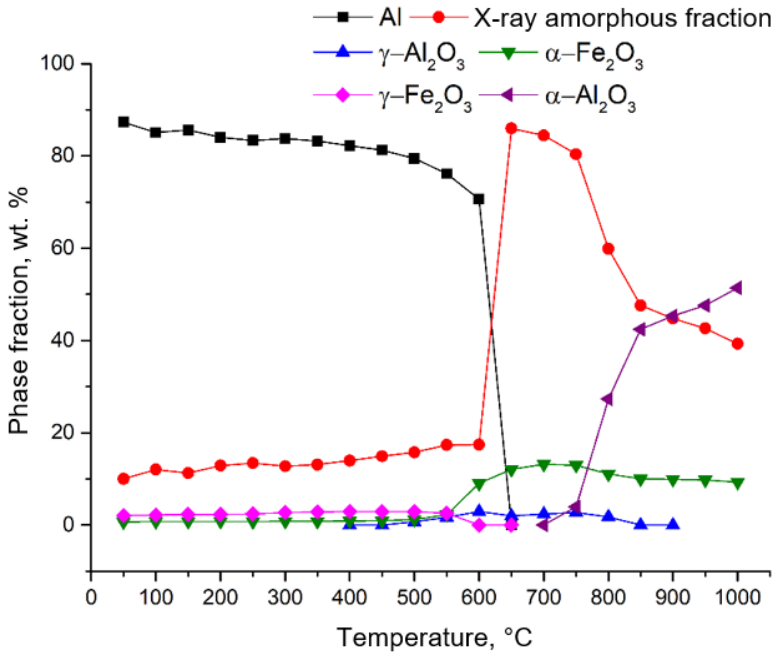

Fig.31. Dependence of the phase composition of the ASD-4 + 10% Fe sample on temperature during heating on air from room temperature to 1000 °C.

According to Fig. 31, about 40% of the X-ray amorphous component corresponds to the amount of liquid Al in the sample at the maximum temperature of X-ray recording (1000 °C). After heating in a resistance furnace at a rate of 10 °C/min to 1000 °C and cooling a similar powder in air to room temperature, full-profile analysis showed the presence of 40% Al in the form of a crystalline phase, 54% α-Al_2O_3, and about 6% hematite (Fe_2O_3). It agrees with the amount of X-ray amorphous phase and α-Al_2O_3 oxide (Fig. 31).

A similar phase formation pattern is characteristic of samples with iron contents of 1 and 5 wt.%. Their diffraction patterns differ in weaker manifestations of iron oxide reflections. An increase in iron concentration leads to a natural decrease in the temperature of the intensive α-Al_2O_3 formation stage due to Al oxidation from 850 °C (1% Fe) to 800 °C (5% Fe) and 750 °C (10% Fe). Moreover, through X-ray diffraction only Al, Al_2O_3 and polymorphic modifications of Fe_2O_3 were detected in the studied modified ASD-4 powder samples. The results presented were obtained for compositions containing modifiers in amounts close to optimal concentrations. It does not lead to a significant reduction in the mass of the main fuel (aluminum).

To establish the patterns of modifier amount influence of iron oxide on the reactivity of ASD-4 aluminum powder, we present the results of oxidation studies. The obtained samples were analysed by thermogravimetry and differential scanning calorimetry during heating in an air environment from room temperature to 1400 °C at a rate of 10 °C/min. The results of thermal analysis are shown as DSC and TG curves in Fig. 32.

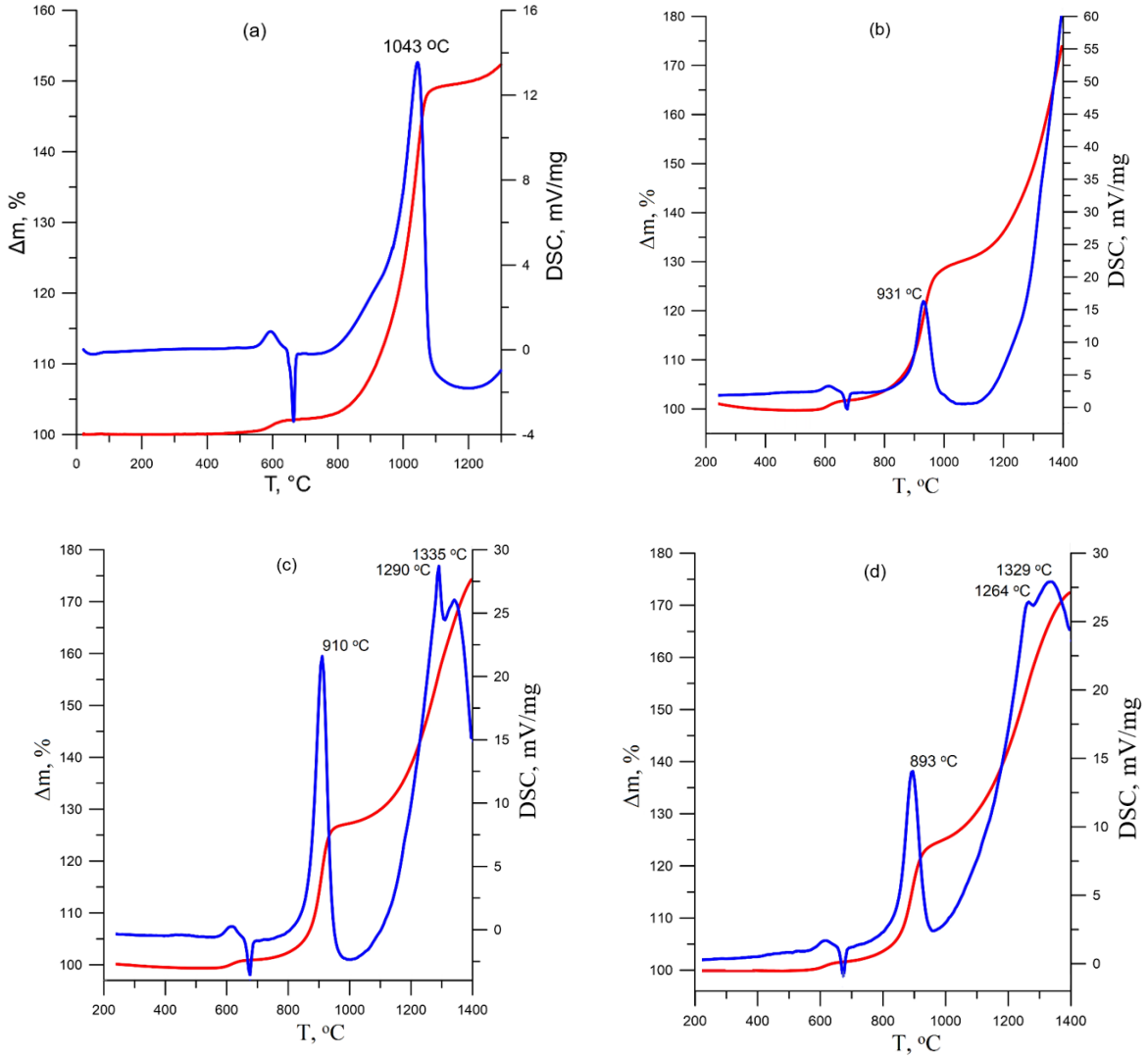

Fig.32. TG and DSC curves of ASD-4 powders: initial (a) and modified with $Fe(OH)(HCOO)_2$ gel: b) Fe_2O_3 = 1 wt.%; c) Fe_2O_3 = 5 wt.%; d) Fe_2O_3 = 10 wt.%.

According to Fig. 32a, the oxidation of aluminum in the modified powder with an iron concentration of 1 wt.% begins below 600 °C and is accompanied by a small exothermic effect. The melting of aluminum (~660 °C) is recorded, followed by an acceleration of mass gain due to oxidation with a maximum heat release at 931 °C and a specific heat of oxidation of 5943 J/g in the range of 800-1060 °C. When the temperature is above 1060 °C, the oxidation process gradually accelerates. However, the formation of a corresponding exothermic peak does not occur up to 1400 °C. With a powder content of 5 wt.% Fe, the intensity of heat release following aluminum melting increases sharply (Fig. 32b). The specific heat of oxidation increases to 7423 J/g; the temperature of the exothermic maximum decreases to 910 °C. With a further temperature increase, a second (1290 °C) and a third (1335 °C) exothermic maximum form. For the sample with a concentration of 10 wt.% Fe, the heat release intensity and the temperature corresponding to the exothermic maximum decrease to 4290 J/g and 893 °C; the positions of the second and third maximum peaks shift slightly to the low-temperature zone (Fig. 32c).

Analysing the results of the studies, amounts of iron oxide additives do not significantly reduce the aluminum content in the powders, activate the oxidation of powdered metallic fuel by atmospheric oxygen. The thermite interaction on the particle surface (peaks on the DSC curves at 931, 920, and 893 °C) increases the specific heat release and the completeness of aluminum oxidation. The ignition temperature of the thermite mixture of composition Al + Fe_2O_3 in vacuum is 965 °C [50].

Conclusion

Figures 1 and 2 present schematics of the oxidation of aluminum particles and powders of Al alloyed with rare-earth metals (REMs). Using the TG, DSC, and X-ray phase analysis data provided in this study, acquired directly during programmed heating in air, and by aligning them along the temperature axis, the oxidation process - comprising sequences of phase formation, phase transitions in oxide layers, and the metallic core - can be represented as a diagram shown in Fig. 1. As an example, Fig. 33 shows a similar diagram for aluminum modified with V_2O_5 and pure Al powder.

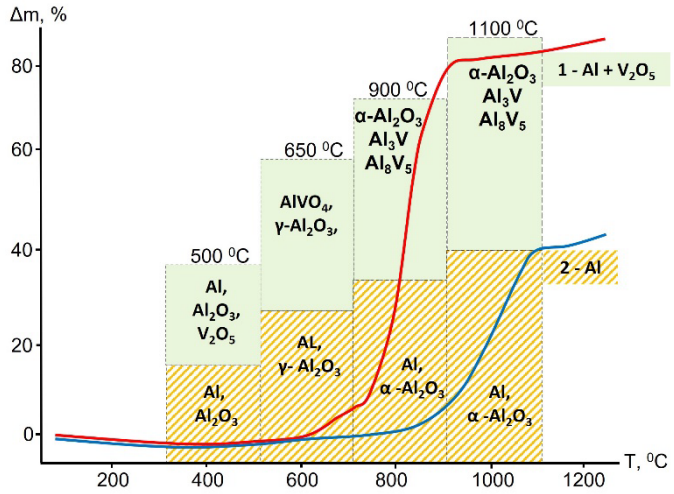

Fig. 33. TG curves of Al-V_2O_5 powder (1) and initial Al (2), and phase formation regions during heating in air at a rate of 10 °C/min.

The thermite interaction between V_2O_5 and Al, the possibility of reactions between oxides, the growth of new crystalline phases in the studied system, interfacial stresses, the availability of synchrotron radiation (SR) and TG/DSC data. etc. allow us to obtain comparative modification results and processes determining the oxidation mechanism in a short time. The combination of the experimental methods considered for justifying the selection of activation pathways for metallic fuel oxidation, existing capability to study model, and real composite formulations of energetic condensed systems (ECS) at the new "SKIF" accelerator will significantly accelerate the development of new high-energy materials.

Funding:

The work was performed in accordance with the state order to the Institute of Solid State Chemistry, Ural Branch, Russian Academy of Sciences, № 124020600007-8.

Conflict of interest:

The authors declare they have no financial or other interests.

References

1. **Pokhil P.F., Belyaev A.F., Frolov Yu.V., Logachev V.S., Korotkov A.I.** Combustion of Powdered Metals in Active Media. Moscow: Nauka, 1972, 294 p. (In Russian).
2. **Alikin V.N., Vakhrushev A.V., Golubchikov V.B., Ermilov A.S., Lipanov A.M., Serebrennikov S.Yu.** Solid Propellants for Rocket Engines. Ed. by Academician A.M. Lipanov. Moscow: Mashinostroenie, 2011, 380 p. (In Russian).
3. **Gromov A.A., Sergienko A.V., Popenko E.M., Slyusarsky K.V., Larionov K.B., Dzidziguri E.L., Nalivaiko A.Y.** Characterization Aluminum Powders: III. Non-Isothermal Oxidation and Combustion of Modern Aluminized Solid Propellants with Nanometals and Nanooxides. *Propellants Exlos. Pyrotech.*, 2020, 45, 1-12. DOI: https://doi.org/10.1002/prep.201900163.
4. **Glotov O.G.** Screening of metal fuels for use in composite propellants for ramjets. *Prog. Aeronaut. Sci.*, 2023, 143, 1-25. DOI: 10.1016/j.paerosci.2023.100954.
5. **Liu Y., Wang Y., Liu Y., Zhao B, Liu W., Yan Q., Fu X.** High calorific values boron powder: ignition and combustion mechanism, surface modification strategies and properties. *Molecules*, 2023, 28, 1-29. DOI: 10.3390/molecules28073209.
6. **Han L., Wang R., Chen W., Wang Z., Zhu X., Huang T.** Preparation and combustion mechanism of boron-based high-energy fuels. *Catalysts*, 2023, 13, 1-16. DOI: 10.3390/catal13020378.
7. **Gopienko V.G.** Metal Powders of Aluminum, Magnesium, Titanium, and Silicon. Consumer Properties and Applications; ed. by A.I. Rudskoy. St. Petersburg: Izd-vo Politekhn. Un-ta, 2012, 356 p. (In Russian).
8. **Korotkikh A.G.** Impact of Aluminum Powder Dispersion on Ignition and Non-Stationary Combustion Processes of Heterogeneous Condensed Systems. Dr. Sci. (Phys.-Math.) Dissertation. Tomsk, 2012, 302 p. (In Russian).
9. **Eselevich D.A.** Study of the Activity and Completeness of Oxidation of Dispersed Aluminum Modified with Surfactants of Various Nature (Ca, Ba, V_2O_5). Cand. Sci. (Chem.) Dissertation. Yekaterinburg, 2015, 121 p. (In Russian).
10. **Kononenko V.I., Shevchenko V.G.** Physical Chemistry of Activation of Disperse Systems Based on Aluminum. Yekaterinburg: UrO RAN, 2006, 238 p. (In Russian).
11. **Shevchenko V.G.** Effect of alloying on the kinetics and mechanism of oxidation of powdered aluminum-based alloys with rare- and alkaline-earth metals. *Combust. Explos. Shock Waves*, 2011, 47, 166-173. DOI: 10.1134/S0010508211020043.
12. **Shevchenko V.G., Volkov V.L., Kononenko V.I., Zakharova G.S., Chupova I.A.** Effect of sodium and potassium polyvanadates on aluminum-powder oxidation. *Combust. Explos. Shock Waves*, 1996, 32(**4**), 436-438. DOI: 10.1007/BF01998494.
13. **Shevchenko V.G., Eselevich D.A., Konyukova A.V., Krasilnikov V.N.** Russian Patent No. 2509790, 2014. (In Russian).
14. **Shevchenko V.G., Eselevich D.A., Konyukova A.V., Krasil'nikov V.N.** Effect of Vanadium Containing Activating Additives on the Oxidation of Aluminum Powders. *Russ. J. Phys. Chem. B*, 2014, 8(**5**), 634-640. DOI: 10.1134/S1990793114050224.
15. **Aulchenko V.M., Evdokov O.V., Kutovenko V.D., Pirogov B.Ya., Sharafutdinov M.R., Titov V.M., Tolochko B.P., Vasiljev A.V., Zhogin I.A., Zhulanov V.V.** One-coordinate X-ray detector OD-3M. *Nucl. Instrum. Methods Phys. Res., Sect. A*, 2009, 603(**1-2**), 76-79. DOI: 10.1016/j.nima.2008.12.164.
16. **Ancharov A.I., Manakov A.Yu., Mezentsev N.A., Tolochko B.P., Sheromov M.A., Tsukanov V.M.** New station at the 4th beamline of the VEPP-3 storagering. *Nucl. Instrum. Methods Phys. Res., Sect. A*, 2001, 470(**12**), 80-83. DOI: 10.1016/S0168-9002(01)01029-4.
17. **Libenson, G.A.** Fundamentals of Powder Metallurgy. Moscow: Metallurgiya, 1975, 200 p. (In Russian).

18. **Antsiferov V.N., Bobrov G.V., Druzhinin L.K.** Powder Metallurgy and Sprayed Coatings. Moscow: Metallurgiya, 1987, 792 p. (In Russian).
19. **Barka D., Weis V.** Powder Metallurgy of Special Purpose Materials. Moscow: Metallurgiya, 1977, 376 p. (In Russian).
20. **Silaev V.A., Putimtsev B.N.** Production of Alloyed Powders by Melt Atomization with Nitrogen. In: Production, Properties and Applications of Metal Powders. Kiev: IPM AN SSSR, 1976, 144 p. (In Russian).
21. **Doronin N.A.** Calcium. Moscow: Gosatomizdat, 1962, 191 p. (In Russian).
22. **Lyakishev P.P.** Phase Diagrams of Binary Metal Systems: Handbook. Vol. 1. Moscow: Mashinostroenie, 1997, 992 p. (In Russian).
23. **Lokshin E.P., Voskoboinikov N.B.** Barium and Its Properties. Apatity: KNTs RAN, 1996, 168 p. (In Russian).
24. **Shevchenko V.G., Latosh I.N., Grigorov I.S., Chupova I.A., Kochedykov V.A.** Role of Intermetallics in the Oxidation of Al-REE System Powders. *Rasplavy [Melts]*, 2009, (**3**), 60-68. (In Russian).
25. **Bykov V.A., Uporov V.B., Sidorov V.E.** Magnetic Susceptibility of Dilute Al-Ce Alloys at High Temperatures. *Rasplavy [Melts]*, 2006, (**6**), 19-24. (In Russian).
26. **Volkovich A.V., Zhuravlev I.S., Trofimov I.S., Gorbachev A.E.** Thermodynamic Properties of Barium in Liquid Alloys with Aluminum and Their Prediction for Alkaline Earth Metals in Other Alloys. *Rasplavy [Melts]*, 2008, (**5**), 16-24. (In Russian).
27. **Shevchenko V.G., Kuznetsov M.V., Bibanaeva S.A., Konyukova A.V., Chupova I.A, Latosh I.N., Kochedykov V.A., Eselevich D.A.** Segregation of calcium on the surface of aluminum-based powders and its effect on oxidation kinetics. *Prot. Met. Phys. Chem. Surf.*, 2012, 48, 631-635. DOI: 10.1134/S2070205112050115
28. **Shevchenko V.G., Eselevich D.A., Ancharov A.I., Tolochko B.P.** Effect of barium on the oxidation kinetics of an aluminum-based alloy powder. *Combust. Explos. Shock Waves*, 2014, 50(**6**) 647-652. DOI: 10.1134/S0010508214060045.
29. **Shevchenko V.G., Krasil'nikov V.N., Eselevich D.A., Konyukova A.V., Ancharov A.I., Tolochko B.P.** Effect of V_2O_5 on the Oxidation Mechanism of ASD-4 Powder. *Combust. Explos. Shock Waves*, 2015, 51(**5**) 572-577. DOI: 10.1134/S0010508215050081.
30. **Krasilnikov V.N., Eselevich D.A., Koniukova A.V., Shevchenko V.G.** Russian Patent No. 2670440, 2018. (In Russian).
31. **Kumar S., Krishnamurthy N.** Synthesis of V-Ti-Cr alloys by aluminothermy co-reduction of its oxides. *Process. Appl. Ceram.*, 2011, 5, 181-186. DOI: 10.2298/PAC1104181K.
32. **Stamatis D., Zhu X., Schoenitz M., Dreizin E.L., Redner P.** Consolidation and mechanical properties of reactive nanocomposite powders. *Powder Technol.*, 2011, 208(**3**), 637-642. DOI: 10.1016/j.powtec.2011.01.002.
33. **Yeh C.L., Wang H.J.** Formation of Ta-Al intermetallics by combustion synthesis involving Al-based thermite reactions. *J. Alloys Compd.*, 2010, 491(**1-2**), 153-158. DOI: 10.1016/j.jallcom.2009.10.203.
34. **Shevchenko V.G., Krasil'nikov V.N., Yeselevich D.A., Konyukova A.V.** Oxidation of Powdered Aluminum after Surface Modification with Mn, Fe, Co, and Ni Formates. *Prot. Met. Phys. Chem. Surf.*, 2019, 55(**1**) 21-27. DOI: 10.1134/S2070205119010210.
35. **Shevchenko V.G., Bulatov M.A., Kononenko V.I., Chupova I.A., Latosh I.N.** Impact of the Properties of the Surface Oxide Layer on the Oxidation of Aluminum Powders. *Powder Metallurgy*, 1988, (**2**), 1-5. (In Russian).
36. **Sharipova N.S., Ksandopulo G.I.** Phase and structural transfomations and mechanism of propagation of self-propagating high-temperature synthesis in a V_2O_5-Al mixture. *Combust Explos Shock Waves*, 1997, 33, 659-668. DOI: 10.1007/BF02671798.
37. **Mear F.O., Louzguine-Luzgin D.V., Inoue A.** Structural investigations of rapidly solidified Mg-Cu-Y. *J. Alloys Compd.*, 2010, 496(**1**), 149-154. DOI: 10.1016/j.jallcom.2010.01.159.
38. **Slobodin B.V., Glazyrin M.P., Fotiev A.A.** Phase Composition of Vanadium-Containing Slags from Steam Generators. *Thermal Engineering*, 1978, (**3**), 40-43 (in Russian).
39. **Woo K.D., Kim J.H., Kwon E.P., Moon M.S., Lee H.B., Sato T., Liu Z.** Fabrication of Al Matrix Composite Reinforced with Submicrometer-Sized Al_2O_3 Particles Formed by Combustion Reaction between HEMM Al and V_2O_5 Composite Particles during Sintering. *Met. Mater. Int.*, 2010, 16, 213-218. DOI: 10.1007/s12540-010-0408-x.

40. **Dabrowska G., Tabero P., Kurzawa M.** Phase relations in the Al_2O_3-V_2O_5-MoO_3 system in the solid state. The crystal structure of $AlVO_4$. *J. Phase Equilib. Diffus.*, 2009, 30(**3**), 220-229. DOI: 10.1007/s11669-009-9503-4.
41. **Shevchenko V.G., Eselevich D.A., Popov N.A., Krasil'nikov V.N., Vinokurov Z.S., Ancharov A.I., Tolochko B.P.** Oxidation of ASD-4 Powder Modified by V_2O_5. *Combust. Explos. Shock Waves*, 2018, 54(**1**), 58-63. DOI: 10.1134/S0010508218010094.
42. **Andrievskii R.A., Khachoyan A.V.** Role of Size Effects and Interfaces in the Physicochemical Properties of Consolidated Nanomaterials. *Russian Journal of General Chemistry*, 2009, 52(**2**), 4-14 (in Russian).
43. **Rusanov A.I.** Colloid-Chemical Aspects of Nanoscience: Nanostructured Materials: Preparation, Properties, Applications. Minsk: Belaruskaya Navuka, 2009, 71-90 (in Russian).
44. A Rietveld extended program to perform the combined analysis: diffraction, fluorescence and reflectivity data using X-ray, neutron, TOF or electrons. Available at: http://maud.radiographema.eu (accessed 10.06.2025).
45. Open-access collection of crystal structures of organic, inorganic, metal-organic compounds and minerals, excluding biopolymers. Available at: http://www.crystallography.net (accessed 12.06.2025).
46. **Ye X., Lin. D., Jiao Z., Zhang L.** The thermal stability of nanocrystalline maghemite Fe_2O_3. *J. Phys. D: Appl. Phys.*, 1998, 31, 2739–2744. DOI: 10.1088/0022-3727/31/20/006.
47. **Duraes L., Costa B.F.O., Santos R., Correia A., Compos J., Portugal A.** Fe_2O_3/aluminum thermite reaction intermediate and final products characterization. *Mater. Sci. Eng. A.*, 2007, 465(**1-2**), 199-210. DOI: 10.1016/j.msea.2007.03.063.
48. **Liu Y., Qian Q., Xu C., Min F., Zhang M.** Synthesis of FeAl/Al_2O_3 Composites by Thermite Reaction. *Asian J. Chem.*, 2013, 25(**10**), 5550-5552. DOI: 10.14233/ajchem.2013.OH14.
49. **Wang Y., Song X.I., Jiang W., Deng G., Guo X., Liu H., Li F.** Mechanism for thermite reactions of aluminum/iron-oxide nanocomposites based on residue analysis. *Trans. Nonferrous Met. Soc. China.*, 2014, 24(**1**), 263-270. DOI: 10.1016/S1003-6326(14)63056-9.
50. **Monogarov K.A., Pivkina A.N., Grishin L.I., Frolov Y.V., Dilhan D.** Uncontrolled re-entry of satellite parts after finishing their mission in LEO: Titanium alloy degradation by thermite reaction energy. *Acta Astronautica*, 2017, 135, 69–75. DOI: 10.1016/j.actaastro.2016.10.031

Received 11.07.2025
Approved 06.08.2025
Accepted 20.08.2025